NATIONAL WATER RESEARCH INSTITUTE

INSTITUT NATIONAL de RECHERCHE sur les EAUX

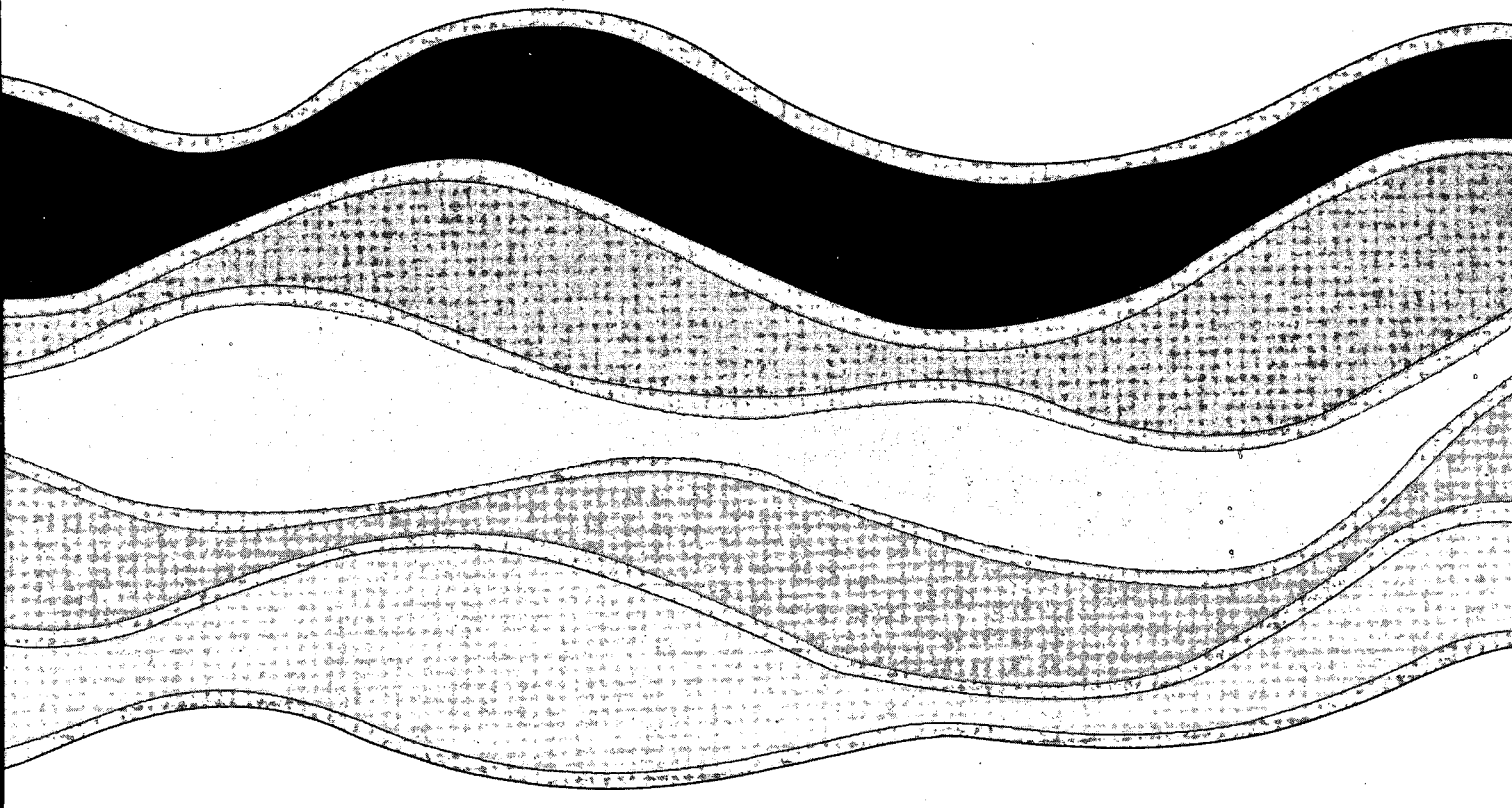

A SIMPLE METHOD FOR CALCULATING THE VELOCITY FIELD BENEATH IRREGULAR WAVES

M. Donelan, F. Anctil and J. Doering

NWRI CONTRIBUTION 91-111

Management Perspective

The accurate prediction of wave-induced velocities is required for the safe engineering design of structures subjected to wave action. This report presents a new theoretically consistent method of predicting the velocity field beneath an irregular wavetrain. A laboratory data set, which provides unique detailed measurements of the velocities near the surface in wave crests, is used to demonstrate the relative accuracy of this new method of prediction. The results show the new method provides more accurate predictions than previously employed prediction methods. This information could help improve designs, thereby reducing the risk of structural failure that might pose an environmental danger.

Dr. John Lawrence
Director
Research and Applications Branch

PERSPECTIVE-GESTION

La prévision exacte des vitesses induites par les vagues est nécessaire pour la conception technique sûre de structures soumises à l'action des vagues. On trouvera dans le présent rapport une nouvelle méthode de prévision du champ de vitesse sous un train d'ondes irrégulier qui est conforme aux données théoriques. Un ensemble de données expérimentales, qui fournissent des mesures détaillées spéciales des vitesses près de la surface dans les crêtes d'onde, est utilisé pour montrer la précision relative de cette nouvelle méthode de prévision. Les résultats montrent que cette méthode permet d'obtenir des prévisions plus précises que les méthodes de prévision utilisées antérieurement. Ces informations permettraient d'améliorer les conceptions, réduisant ainsi le risque de défaillance des structures qui peut éventuellement constituer un danger pour l'environnement.

M. John Lawrence
Directeur
Direction de la recherche pure et appliquée

A SIMPLE METHOD FOR CALCULATING THE VELOCITY FIELD BENEATH IRREGULAR WAVES

M. Donelan, F. Anctil†, and J. Doering

National Water Research Institute
Canada Centre for Inland Waters
Burlington, Ontario
Canada, L7R 4A6

Abstract

The need for estimating water velocities beneath ocean waves for engineering calculations has produced *ad hoc* methods that are based on the relation between sea surface elevation and the velocity potential given by linear theory. These methods depend on some assumptions, which are, in general, clearly inappropriate for ocean waves. In this paper, we present a new, theoretically consistent method of superposition for a spectrum of linear waves and examine its characteristics with respect to several existing methods. Numerical simulations and laboratory data, collected using a surface-following device and an acoustic current meter, are used to test the relative and absolute accuracy of the new method and four existing methods of predicting wave-induced velocities.

Résumé

Des méthodes spéciales fondées sur le rapport entre l'élévation du niveau de la mer et le potentiel de vitesse donné par la théorie linéaire ont été mises au point en raison de la nécessité d'évaluer la vitesse de l'eau sous les vagues océaniques à des fins de calculs techniques. Ces méthodes reposent sur certaines hypothèses, qui sont, en général, tout à fait inappropriées pour les vagues océaniques. Dans le présent article, les auteurs présentent une méthode nouvelle, conforme aux données théoriques, de superposition dans le cas d'un spectre de vagues linéaires, et étudient ses caractéristiques par rapport à plusieurs méthodes existantes. Des simulations numériques et des données de laboratoire, obtenues à l'aide d'un dispositif escorteur et d'un courantomètre acoustique, sont utilisées pour vérifier la précision relative et absolue de la nouvelle méthode ainsi que de quatre méthodes existantes de prévision des vitesse induites par les vagues.

† Université Laval, Département de Génie Civil, Sainte Foy, Québec, Canada, G1K 7P4

1. Introduction

Engineering calculations of wave induced forces on coastal and offshore structures require a precise knowledge of the flow kinematics. The usual basis for such calculations is the Morison equation (Morison *et al.*,1950), in which the principal force components are due to drag and inertial forces; the first is approximately proportional to fluid speed squared and the second to local fluid accelerations in the Reynolds number ranges of usual engineering interest. The calculated drag force is thus especially sensitive to errors in speed estimates in regions of high flow speeds, such as those near and in particular above the mean water level (mwl). On the other hand, the calculated inertial forces are relatively sensitive to the high frequency (short wave length) end of the spectrum, and the flow due to the short waves attenuates quickly with depth.

A substantial body of work has been devoted to finding reliable ways of estimating the flow field beneath a natural wind-generated wave field (Reid, 1958; Wheeler,1969; Forristall,1981; Lo and Dean,1986; Rodenbusch and Forristall,1986). However, there is no generally accepted method of proven accuracy. Much of the work finds its foundation in the success of the linear Gaussian model; that is, the idea that the surface elevation may be viewed as the linear superposition of an infinite sum of infinitesimal waves independently propagating in random directions. Such a model has served the engineering community fairly well in yielding reliable estimates of, for example, the probability distribution of heights (Longuet-Higgins, 1952) and, more recently, of the joint distribution of heights and periods (Arhan *et al.*, 1976: Longuet-Higgins, 1983), and the length of a run of waves exceeding a particular height (Ewing, 1973). Such estimates of the statistics of the surface elevation have been used to set design parameters based on the highest expected wave or on group lengths. The procedure for establishing limits on the statistics of heights, periods and run lengths, based on a Gaussian distribution of linear waves, appears to be adequate for engineering purposes. Higher order corrections based on non- linearity in the wave field (Huang *et al.*, 1984), and on wave breaking criteria (Tayfun, 1981) are generally small and not included in engineering calculations.

Once the design criteria, based on expected heights, periods, and runs of waves have been set, the engineer is then faced with the problem of establishing corresponding flow fields for the calculations of expected forces and the consequent establishment of structural criteria. It is here that one finds that there is no standard method of establishing the concomitant wave kinematics, that there are substantial differences between methods, that many proposed methods are based on arbitrary adjustments to theory, and that there are very few data sets for testing the various methods near and above the mean water level. In particular, it is above the mean water level where the flow is most intense and the drag more (quadratically) so, and where the short waves enhance the flow accelerations and hence the inertial forces.

It is the purpose of this paper to develop a method of establishing the flow kinematics at any point beneath a given arbitrary surface based on application of linear theory in a natural manner without recourse to arbitrary assumptions. Furthermore, the method is tested using numerical simulations and data acquired very near the surface of a mechanically driven wave field using an

electro-hydraulic surface-follower and an acoustic current meter. In the following section (§2) the existing methods are reviewed. The new method is described in §3 and compared to the existing methods in §4. A description of the laboratory experiments follows in §5. The discussion and conclusions follow in §6 and §7, respectively.

2. Existing Methods: A review

The main advantage of linear theory over non-linear ones is the potential to superimpose an infinite sum of wave harmonics, each with its own amplitude, frequency, phase and direction, to simulate a natural irregular sea. Thus, one can describe the water surface displacement by

$$\eta(x,y,t) = \sum_{m=1}^{M}\sum_{n=1}^{N} a_{mn}\cos(k_{m_x}x + k_{m_y}y - \omega_m t + \epsilon_{mn}), \tag{1}$$

where $a_{mn} = \sqrt{2S(\omega_m,\theta_n)\Delta\omega_m\Delta\theta_n}$ is an amplitude, S is a real or simulated directional frequency spectrum, ω is some frequency, θ is a direction, k is a wavenumber, x and y are horizontal coordinates, t is time, and ϵ is a real or simulated random phase. m and n denote the various components of the spectrum. In the absence of Doppler shifting the wavenumber and the radian frequency are related by the dispersion relation, *i.e.*,

$$\omega_m^2 = gk_m\tanh(k_m h), \tag{2}$$

where h is the water depth and g the acceleration due to gravity. The wave kinematics are readily derived from the corresponding velocity potential, *viz.*,

$$\phi(x,y,z,t) = -\sum_{m=1}^{M}\sum_{n=1}^{N}\frac{a_{mn}\cosh k_m(h+z)}{\omega_m\cosh k_m h}\sin(k_{m_x}x + k_{m_y}y - \omega_m t + \epsilon_{mn}), \tag{3}$$

where z is the vertical coordinate, which is taken here to be positive above the mean water level. From (3) the two (orthogonal) horizontal velocities and the vertical velocity are given by,

$$\frac{\partial\phi}{\partial x} = u(x,y,z,t) \tag{4a}$$
$$= \sum_{m=1}^{M}\sum_{n=1}^{N} a_{mn}\omega_m\frac{\cosh k_m(h+z)}{\sinh k_m h}\cos(k_{m_x}x + k_{m_y}y - \omega_m t + \epsilon_{mn})\cos(\theta_n),$$
$$\frac{\partial\phi}{\partial y} = v(x,y,z,t) \tag{4b}$$
$$= \sum_{m=1}^{M}\sum_{n=1}^{N} a_{mn}\omega_m\frac{\cosh k_m(h+z)}{\sinh k_m h}\cos(k_{m_x}x + k_{m_y}y - \omega_m t + \epsilon_{mn})\sin(\theta_n),$$
$$\frac{\partial\phi}{\partial z} = w(x,y,z,t) \tag{4c}$$
$$= \sum_{m=1}^{M}\sum_{n=1}^{N} a_{mn}\omega_m\frac{\sinh k_m(h+z)}{\sinh k_m h}\sin(k_{m_x}x + k_{m_y}y - \omega_m t + \epsilon_{mn}).$$

One of the assumptions inherent in the derivation of linear theory is the free surface boundary condition is applied at the mwl and not at the actual free surface. Thus, the theory can only be successful when dealing with waves of small amplitude. Fourier decomposition of a wave field into its many frequency components should satisfy this requirement.

Using equations (4a-c), the wave kinematics at any given time and position can be found very easily if one follows the work of Reid (1958), and assumes that the formula holds for points significantly above the mwl. All wave components are then considered independent of one another, which implies that the vertical surface coordinate of a high-frequency component superimposed upon a lower one is the sum of both components (figure 1). The contribution of the high-frequency component to the velocity field is exaggerated by an increased vertical displacement. Velocities reach a maximum near the surface, so the application of linear superposition in this area leads to considerable over estimation. On the other hand, away from the surface, beneath the mwl, the theory has compared favorably with both laboratory and field data (Dean and Perlin, 1986). Reasonable agreement occurs at depth because the contribution of the high-frequency components decays rapidly with depth.

Wheeler (1969) was the first to propose an alternate method, known as coordinate stretching or simply stretching, for the evaluation of velocities above the mean water level in wave crests. The vertical coordinate transformation that he proposed is

$$z = \frac{h(z' - \eta)}{h + \eta}, \tag{5}$$

where z' is the desired location of kinematic evaluation. This "intuitive" approach implies that the surface velocities in a stretched system are equivalent to those at the mwl of an unstretched system. Thus, the velocity exaggeration near the surface that was previously described is avoided. However, both laboratory and field data (Forristall, 1981) show that the method tends to underpredict velocities above the mwl.

Using data obtained from the Ocean Test Structure field experiment, Forristall (1981) proposed a different modification to linear theory. His modification assumes a linear variation of velocity above the mwl. In particular, linear theory is used up to mwl, but subsequent values are extrapolated upward using the vertical gradient of velocity at the mwl. The formulation is a truncated Taylor series (Rodenbusch and Forristall, 1986), with a constant vertical partial derivative, *i.e.*,

$$u(x,y,z,t) = u(x,y,0,t) + z\left.\frac{\partial u(x,y,0,t)}{\partial z}\right|_{z>0}. \tag{6}$$

The error associated with this method is proportional to the size of z. The method is typically found to overpredict other data sets.

Noting that observations tend to lie somewhere between these two approaches, Rodenbusch and Forristall (1986) further proposed an another method called delta-stretching. This method fits the data by interpolating between the predictions of extrapolation and stretching. Clearly, all three methods are *ad hoc* adjustments to fit linear theory to real data.

Yet another modification to linear theory has been proposed by Lo and Dean (1986), who applied the free surface boundary condition at the free surface and not at the mwl; this method was suggested earlier by Chakrabarti (1971) in the discussion of a paper. Lo and Dean obtained a modified stretching factor, of the form $\cosh kh / \cosh k(h+\eta)$, which affects the velocity potential, and gives the following formulations for the horizontal and vertical velocities:

$$u(x,y,z,t) = \sum_{m=1}^{M}\sum_{n=1}^{N} a_{mn}\omega_m \frac{\cosh k_m(h+z)}{\sinh k_m(h+\eta)} \cos(k_{m_x}x + k_{m_y}y - \omega_m t + \epsilon_{mn})\cos(\theta_n), \tag{7a}$$

$$v(x,y,z,t) = \sum_{m=1}^{M}\sum_{n=1}^{N} a_{mn}\omega_m \frac{\cosh k_m(h+z)}{\sinh k_m(h+\eta)} \cos(k_{m_x}x + k_{m_y}y - \omega_m t + \epsilon_{mn})\sin(\theta_n), \tag{7b}$$

$$w(x,y,z,t) = \sum_{m=1}^{M}\sum_{n=1}^{N} a_{mn}\omega_m \frac{\sinh k_m(h+z)}{\sinh k_m(h+\eta)} \sin(k_{m_x}x + k_{m_y}y - \omega_m t + \epsilon_{mn}). \tag{7c}$$

The dispersion relation is affected by this factor and now has a functional dependence on the water surface displacement,

$$\omega_m^2 = g k_m \tanh k_m(h+\eta). \tag{8}$$

The effects of non-linearities, such as those associated with shoaling, are not addressed by any of the previous methods. The application of these methods should therefore be restricted to deep water. While still retaining the principle of superposition, such nonlinear terms (effects) are considered by Sharma and Dean (1979), Gudmestad and Connor (1986), Koyoma and Iwata (1985), and Gudmestad (1990).

Finally, Forristall (1985, 1986) has also proposed a model for predicting near surface velocities using a model based on kinematic boundary condition fitting. The model does not use superposition procedures but evaluates velocities under any specified surface, through the numerical calculation of the potential function. When extended to two-dimensional waves, this method has to be implemented on a large computer, and consequently will not be considered any further herein.

3. A New Method: Superposition

The new method proposed here is based on the linear superposition of a sum of freely propagating wavetrains. It is assumed that shorter waves ride on longer ones, so that the mean surface seen by a particular wave component is given by the linear superposition of all the longer wave components and has the surface velocity commensurate with that. The addition of successively shorter wave components, therefore, alters the surface elevation and changes the flow field in accordance with linear theory applied to the new component about the existing (sum of all longer components) surface.

A step by step procedure for computing the flow field at the nodes of an arbitrarily fine grid is outlined below.

Step 1. A time series of surface elevation, $\eta(t)$, of irregular waves (real or simulated) is Fourier transformed. All the Fourier components (a_{mn} and ϵ_{mn}) are retained.

Step 2. A grid of desired resolution is constructed, such that the grid extends well above the highest value of $\eta(t)$ and down to a level of near zero motion; generally a depth corresponding to approximately one half the wavelength of the spectral peak.

Step 3. $\eta(t)$ is reconstructed in stages by adding successive mn components. At each stage the velocity field for a specific component is computed at all depths in the region, *viz.*,

$$-\frac{\pi}{k_{mn}} + \tilde{\eta}_{mn-1} < z < \eta_{mn} + \tilde{\eta}_{mn-1}, \tag{9}$$

where η_{mn} is the surface elevation for a specific (Fourier) component and $\tilde{\eta}_{mn-1}$ is the sum of the Fourier components of surface elevation up to and including the preceding component. Note, the region of velocity computation varies with the addition of each successive component. This incremental velocity field (*viz.*, $u_{mn}(t), v_{mn}(t), \text{and} w_{mn}(t)$), evaluated from (4), is added to the velocity field from the sum of all the previous components at all grid points. The values of the new velocities at the new surface are then given to all grid points above the new surface. This is a computationally convenient way of reflecting the premise that the short waves ride on the longer ones, while allowing for changes in the surface position at every step.

Step 4. Upon completion of step 3 the original surface elevation $\eta(t)$ will have been recovered and the velocity field beneath the surface will have been determined. It remains only to set all velocities above the surface to zero to complete the required description of the wave-induced velocity field.

The Fourier decomposition of a time series of surface elevation at a point yields the "frequency of encounter" Ω_m of each wave component and not its intrinsic frequency ω_m, which is needed to compute the wavenumber k_{mn} from the dispersion relation. This complication arises because the separate wave components are not propagating on still water but may be carried along by a current $\underline{U}$ or the surface orbital velocities of longer components $\underline{\tilde{u}}_{mn-1}\big|_{z=\tilde{\eta}_{mn-1}}$ (Phillips, 1977). Hence,

$$\Omega_m = \omega_m + k_{mn}(\underline{U} + \underline{\tilde{u}}_{mn-1}\big|_{z=\tilde{\eta}_{mn-1}}), \tag{10}$$

where the underline denotes a vector. Thus, contributions to a given Ω_m arise from different wavelengths on different parts on the underlying surface $\tilde{\eta}_{mn-1}$. However, the surface velocity $\underline{\tilde{u}}_{mn-1}$ is known at each step and provided the current is also known or small, ω_{mn} may be evaluated (by successive approximations) at each column in the grid and the analysis continued as in the previous section. Further discussion of Doppler shifting is left till the following section.

4. Comparison of the methods

The method proposed in the previous section is compared with the four methods outlined in §2: direct linear (Reid, 1958), stretching (Wheeler, 1969), extrapolation (Forristall, 1981) and modified stretching (Lo and Dean, 1986). This comparison is performed using simulated time series constructed from a strongly forced deep water directional DHH spectrum (Donelan *et al.*, 1985). A strong wind forcing parameter is used in these simulations, in order to obtain steep waves that enhance the differences between the methods.

Figure 2 presents an isometric view of a DHH directional spectrum, defines the wind forcing parameters, peak frequency selected, and gives the resultant significant wave height and maximum spectral value at the peak. The wave frequency varies from 0.25 to 2 rad/s in increments of 0.05, and the direction from $-\pi$ to π in increments of $\pi/12$. The mean direction of this spectrum is 0°. The water depth is 50 m, so the peak of the spectrum which is centered at 0.70 rad/s ($\approx$ 0.11 Hz), falls just inside the intermediate depth water region ($^{d}/_{L} \approx 0.4$).

Time series of surface displacement (η) and horizontal velocity ($u\big|_{z=\eta}$) for each method are presented in Figure 3a. The similarity between the surface elevation and the computed velocities is obvious. The largest discrepancy between the predictions by the various methods occurs at the extrema, namely, the crests and troughs. Figure 3b shows an enlargement of the wave that is centered at $\approx$ 34 s in Figure 3a. No difference is detectable between the predictions due to the stretching and modified stretching methods, since both methods lead to the same equation at the surface of deep water waves; they also lead to very similar equations in intermediate depth water. The predictions arising from the proposed method closely follow those from the stretching methods, but are slightly higher in the crest and lower in the trough. The predictions from the direct linear and extrapolation methods behave differently from the others and generally give substantially higher values in the crest and much lower values in the trough. Note that the forward face of the wave-induced velocity predicted by the direct linear method (Figure 3b) does not closely resemble the surface elevation as does the proposed method and the two stretching methods because the high frequency components are exaggerated in this method.

The orthogonal component of horizontal velocity (v) along the minor axis and the vertical velocity (w) are not presented here because the agreement between the methods is quite close. v is, of course, smaller than u since the mean direction (major axis in velocity) of the spectrum is along u. The vertical velocity w reaches a maximum for a given wave when the surface displacement is at the mwl, which is where the discrepancies between the predicted values of u are typically quite small.

Figure 4 shows the variation of the horizontal velocity u with depth under the crest of the wave that is shown in figure 3b. The highest predicted velocities are derived from the direct linear method, and increase exponentially above the mwl. Although, the method of extrapolation is intended to prevent such a rapid increase it is only partially successful in this regard. On the other hand, the modified stretching method gives the lowest values at all depths, and produces similar results to the stretching method at the surface. The proposed method predicts higher velocities

than either of the stretching methods, but substantially lower values than either of the linear or extrapolation methods.

Predictions obtained using the method of superpositon were re-examined to determine the sensitivity of the method to Doppler shifting. Incorporating this effect significantly increases the computational complexity because now the wavenumber depends on the directional characteristics of the free surface spectrum. Moreover, the resulting expression for wavenumber is quadratic. To select the "correct" root Jonsson *et al.* (1970) have suggested using the root, which for small currents, tends without discontinuity to the value obtained for no current. However, when the previous results were repeated to account for the effects of Doppler shifting, the differences observed were very small. In light of the small differences and significant increase in computational time, accounting for the effects of Doppler shifting does not appear to be worth while.

The sensitivity of the predictions by the five methods to bandwidth was also examined. The bandwidth was varied by a factor of 16 by using 2048 through to 128 points in each FFT block. Stretching, modified stretching, and superposition showed no significant differences in their respective predicted values for this range of FFT block sizes. The effect of bandwidth on the predictions obtained using extrapolation and linear theory is less clear since these methods tend to overpredict.

5. Laboratory Experiments

Laboratory experiments at a scale of 1:10 were conducted in NWRI's 100 m flume. Irregular wave generation software developed by the National Research Council Canada (Funke and Mansard, 1984), was used to generate DHH target spectra. Two peak periods (0.9 and 0.6 Hz) and two peak enhancement or wave age values were selected, (U/c_p = 0.83 (fully developed) and 5.0 (strongly forced)). A still water depth of 1.0 m was used for all runs. A summary of the runs and the parameters used for each run is given in table 1.

Measurements of the near surface velocity were obtained using a surface-following device and a current meter. The surface-follower is an electro-hydraulic device whose position is controlled by a feedback loop involving a surface intersecting capacitance-type wave staff, a signal conditioner, and a Moog servovalve. A photograph of the surface-follower with the current meter is shown in figure 5. An indication of how well this instrument follows the water surface is shown in figure 6a. A more general indication of the overall system response is the transfer function of the system, which is shown in figure 6b. This response function was obtained by injecting sine waves of different frequencies into the (normal) feedback loop. The superposition of a signal generator sine wave on the output signal from the surface intersecting gauge causes the surface-follower to move the surface intersecting gauge with respect to the still water surface so that its output continuously offsets the sine wave introduced by the signal generator. A cross-spectral analysis between driving signal frequencies and the surface intersecting gauge yields the transfer function shown for the surface-follower.

The current meter, which was mounted on the end of the surface-follower, is a Minilab SD-12 3-axis, acoustic flow meter manufactured by Sensordata a.s, in Bergen, Norway. The current meter

was calibrated using the tow tank calibration facility at NWRI. The x-y axes of the current meter where calibrated at four tow speeds (0.2, 0.4, 0.6, 0.8 m/s) in 15° steps to obtain the horizontal cosine response. Figure 7a shows the along axes response for the x and y channels, which was used as the reference gain response for the cosine response shown in figure 7b. The degree of linearity and the good cosine response exhibited by this instrument are indicative of the data quality.

The analog signals of colocated surface elevation, velocity, and depth of immersion (*i.e.*, the signal from the surface intersecting gauge on the follower) were lowpass filtered at 10 Hz then sampled digitally at 20 Hz. Corrections were made to the current meter data for the 2 Hz end-stage filter in the current meter electronics and for the sine cardinal response associated with spatially averaging along a 3 cm horizontal acoustic path length. Following these corrections, all data were subsequently lowpass filtered (using FFT truncation) at 3.33 Hz, then decimated to 6.66 Hz for computational purposes.

A similar data set was recently collected by Klinting and Jacobsen (1990) and compared to second-order wave theory.

6. Discussion: Data vs Methods of Prediction

Eight laboratory runs were selected for comparison with the five previously outlined methods of velocity prediction. A summary of the parameters used for each of these runs is given in table 1. Three of the eight runs, 188, 191, and 196 are considered in detail. The same wavetrain ($T_p = 1.66$ s, $U/c_p = 5.00$) was used for runs 188 and 196, however, the velocity measurements were made at different depths (46 and 126 mm, respectively). This wavetrain is the largest and steepest of those generated. Run 191 on the other hand is a fully developed deep water wavetrain and provides a contrast to the strongly forced intermediate depth wavetrain used for runs 188 and 196.

Table 2 summarizes the measured rms deviation, normalized skewness, and kurtosis, and those predicted using all five methods for all eight runs. By inspection it is clear that the rms of the velocity field is best predicted by the method of superposition, which consistently underpredicts by approximately 0.6 to 9%. The predictions by stretching and modified stretching are also quite close, but are consistently less than those from superposition. The methods of extrapolation and linear theory overpredict the near surface measurements ($z - 0.46$ m), but closely predict those deeper down ($z = -0.126$ m).

A more sensitive (statistical) indication of the ability of these methods to predict accurately the wave-induced velocity is given by a comparison of the skewness and kurtosis predictions. It is well-known that a Gaussian process has zero skewness, but a finite length record of a Gaussian process would have a small skewness. However, the measured values in table 2 indicate that the measured skewness of these velocity fields is distinctly nonzero. The positive skewness exhibited by these records indicates that the velocity induced by the passage of a wave crest is stronger than that induced by the passage of a wave trough, suggesting a Stokes-like shape. This tendency can be clearly seen in a segment of the measured time series for runs 188, 191, and 196, shown by the solid line in figures 8(a-c), respectively. For the measurements closest to the surface (runs 188, 189, 190, and 191) superposition overpredicts the skewness by approximately 40%, whereas the stretching

methods underpredict runs 189-191 and overpredict run 188. The overprediction of skewness by these methods is evident in figure 8(a). Both methods tend to predict closely the crest velocities but notably underpredict the velocities in the troughs. The deeper measurements, however, are underpredicted by both stretching methods by more than twice as much as those by superposition. The methods of extrapolation and linear theory grossly overpredict skewness at both of the depths considered.

With only one exception, run 188, the kurtosises of the measured data are greater than 3.00, indicating a non-Gaussian character. The large kurtosis predictions from extrapolation and linear theory reflect the fact that these methods grossly overpredict crest velocities.

Figures 9(a-d) show scatter plots of the measured velocities versus those predicted using the methods of superposition, stretching, modified stretching, and extrapolation, respectively, for run 188 (recall, T_p = 1.66 s, U/c_p = 5.00 (strongly forced), and z = −46 mm). Although there is a tendency for superposition to underestimate the velocities in the troughs (negative velocities) slightly more than stretching or modified stretching, the rms error of the superposition predictions is about 1% less than those for the stretching methods (see table 3), suggesting slightly better predictions over the remainder of each wave. Extrapolation (figure 9d) clearly, overpredicts the crest velocities and underpredicts the trough velocities, yielding an rms error more than twice as large as the previous methods. Linear theory, which is not shown, provides the worst predictions of all, with an rms error nearly two orders of magnitude larger than that for superposition.

Figure 10 shows that the measurements at z = −126 mm from mwl (run 196), yields velocities that are comparable in magnitude to those observed at z = −46 mm (figure 9). The relative accuracy of the methods as measured by the rms error remains the same, but the absolute error decreases slightly, indicating slightly closer predictions by all methods at depth. At this depth both stretching methods significantly underpredict the velocities under the crests, while superposition closely follows the measured velocities.

For a fully developed, less steep spectrum of waves (run 191), the near surface predictions (z = −46 mm) by each of the four methods is similar (figures 11a-d). Extrapolation tends not to overpredict as much as for the steep waves used for runs 188 and 196. There is also less tendency for superposition to underpredict the trough velocities.

The spectra of the measured and predicted velocities for runs 188, 191, and 196, figures 12(a-c) respectively, show that both the method of superposition and stretching slightly underpredict the amplitude of the fundamental or peak frequency, whereas the amplitude of the long waves is significantly underpredicted. On the high frequency side the calculations generally underestimate the measurements, but superposition lies closer to the measurements than stretching. At the highest frequencies the current meter undoubtably responds to turbulence (possibly induced by its presence in the flow), whereas the methods of calculation do not.

7. Conclusions

Linear methods can provide close predictions of wave-induced velocities at depth and close to the surface. A comparison of four existing velocity prediction methods, *viz.*, stretching, modified

stretching, extrapolation, and linear theory, to a new method of prediction, which is called superposition, shows that the predictions from stretching, modified stretching, and superposition are quite close. Extrapolation and linear theory on the other hand tend to grossly overpredict the crest velocities. A comparison of the rms errors and spectral response for superposition, stretching, and modified stretching, indicates that superposition is slightly better overall. The advantage of the new method of superposition over existing methods is it is based on linear theory without recourse to arbitrary assumptions.

An important difference between the methods is in their prediction of mean Eulerian and Lagrangian drift velocities under irregular waves. It is easily seen that the stretching methods force the surface Lagrangian drift to zero and predict negative Eulerian drift at all fixed depths beneath the lowest troughs. The new method, on the other hand, gives no net Eulerian drift and a positive Lagrangian drift is demanded by theory. The need for correct estimates of wave drift as important in models for predicting iceberg trajectories, mooring dynamics, and oil spill migration.

Acknowledgments

The authors wish to thank Drs. W. Drennan, K. Kahma, and E. Terray for their helpful discussion and insight. Dr. M. Skafels' comments on this manuscript are very much appreciated. The technical support of Messrs. G. Voros, K. Davis, and T. Nudds is greatly appreciated. Financial support for F. Anctil was provided by the Natural Science and Engineering Research Council (NSERC) of Canada. Dr. J. Doering expresses his gratitude to the the Panel for Energy Research and Development (PERD) for their financial support, task 6.2, study 62124.

References

Arhan, M., Cavanie, A. and Ezraty, R., 1976. Relation statistique entre hauteur et période de vagues de tempête. C.R. Acad. Sc. Paris, B189:189-192.

Chakrabarti, S.K., 1971. Dynamics of single point mooring in deep water. Discussion: J. Water Harbour Coastal Engr. Div., ASCE, 97(WW3):588-590.

Dean, R.G. and Perlin, M., 1986. Intercomparison of near bottom kinematics by several wave theories and field and laboratory data. Coastal Eng., 9:399-437.

Donelan, M.A., Hamilton, J. and Hui, W.H., 1985. Directional spectra of wind-generated waves. Phil. Trans. R. Soc. Lond., A315: 509-562.

Ewing, J., 1973. Mean length of runs of high waves. J. Geophys. Res., 78(C12):1933-1936.

Forristall, G.Z., 1981. Kinematics of directionally spread waves. Proc. Conf. on Directional Wave Spectra Applications, ASCE, Berkeley, 129-146.

Forristall, G.Z., 1985. Irregular wave kinematics from a kinematic boundary condition fit (KBCF). Applied Ocean Research, 7(4):202-212.

Forristall, G.Z., 1986. Kinematics in the crests of storm waves. Proc. 20th Conf. on Coastal Eng., ASCE, Taipei, 208-222.

Funke, E.R. and Mansard, E.P.D., 1984. The NRCC "random" wave generation package. Tech. Report, TR-HY-002, NRCC no. 23571, 78 p.

Gudmestad, O.T. and Connor, J.J., 1986. Engineering approximations to nonlinear deep water waves. Appl. Ocean Res., 8(2):76-88.

Gudmestad, O.T., 1990. A new approach for estimating irregular deep water wave kinematics. Appl. Ocean Res., (in press).

Huang, N.E., Long, S.R., Bliven, L.F., and Tung, C.C., 1984. The non- Gaussian joint probability density function of slope and elevation for a nonlinear gravity wave field. J. Geophys. Res., 89(C2):1961-1972.

Jonsson, I.G., Skougaard, C., and Wang, J.D., 1970. Interaction between waves and currents. Proc. 12th Conf. on Coastal Eng., ASCE, Washington, D.C., 489-507.

Klinting, P. and Jacobsen, P., 1990. Near surface wave irregular wave kinematics. In *Water Wave Kinematics*, Tørum and Gudmestad (editors), Kluwer Academic, 185–200.

Koyama, H. and Iwata, K., 1985. Estimation of water particle velocities by a modified transfer function method. Coastal Eng. in Japan, 28:1-13.

Lo, J.M. and Dean, R.G., 1986. Evaluation of a modified stretched linear wave theory. Proc. 20th Conf. on Coastal Eng., ASCE, Taipei, 522-536.

Longuet-Higgins, M.S., 1952. On the statistical distributions of the heights of sea waves. J. Mar. Res., IX(3):245-266.

Longuet-Higgins, M.S., 1983. On the joint distribution of wave periods and amplitudes in a random wave field. Proc. R. Soc.Lond., A389:241-250.

Morison, J.R., O'Brien, M.P., Johnson, J.W. and Schaaf, S.A., 1950. The force exerted by surface waves on piles. Petroleum Transaction, AIME,189. 149-154.

Phillips, O.M., 1977. The dynamics of the upper ocean. Cambridge University press. 336 p.

Reid, R.O., 1958. Correlations of water level variations with wave forces on a vertical pile for non-periodic waves. Proc. 6th Conf. on Coastal Eng. 749-786.

Rodenbusch, G. and Forristall, G.Z., 1986. An empirical model for random directional wave kinematics near the free surface. Proc. Offshore Technology Conf., Houston, OTC 5097, 137-146.

Sharma, J. and Dean, R.G., 1979. Second-order directional seas and associated wave forces. Proc. Offshore Technology Conf., Houston, OTC 3645, 2505-2514.

Tayfun, M.A., 1981. Breaking limited wave heights. J. Waterway Port. Coastal Ocean Engr. Div., ASCE, 107(WW2):59-69.

Wheeler, J.D., 1969. Method for calculating forces produced by irregular waves. Preprints Offshore Technology Conf., Houston, OTC 1006, 71-82.

Table 1-Data Summary

Spec. Type	U/c_p	T_p [s]	H_c [m]	z [m]	Run No.
DHH	0.83	1.66	0.142	-0.046	189
				-0.126	197
		1.11	0.072	-0.046	191
				-0.126	199
	5.00	1.66	0.237	-0.046	188
				-0.126	196
		1.11	0.115	-0.046	190
				-0.126	198

Note, the SWL for all runs was 1.0 m.

Table 2-Summary of Statistics

Run	Quantity	Measured	Super.	Stret.	M.Stret.	Extrp.	Lin.
188	rms	0.263	0.252	0.248	0.248	0.304	2.585
	skew.	0.411	0.651	0.465	0.350	2.309	21.67
	kurt.	2.911	3.508	3.235	3.129	15.96	480.9
189	rms	0.181	0.176	0.171	0.170	0.206	0.316
	skew.	0.478	0.703	0.433	0.371	2.412	11.01
	kurt.	3.193	3.792	3.083	2.979	17.88	188.3
190	rms	0.159	0.158	0.150	0.150	0.182	0.194
	skew.	0.779	0.885	0.530	0.486	1.876	2.582
	kurt.	4.245	4.257	3.486	3.407	9.260	16.10
191	rms	0.099	0.098	0.093	0.093	0.107	0.108
	skew.	0.685	0.968	0.549	0.513	1.774	1.920
	kurt.	4.126	5.021	3.660	3.572	9.678	11.01
196	rms	0.239	0.219	0.210	0.210	0.249	0.340
	skew.	0.502	0.602	0.291	0.119	2.157	9.310
	kurt.	3.145	3.605	2.806	2.706	16.85	151.3
197	rms	0.149	0.141	0.136	0.136	0.148	0.148
	skew.	0.638	0.532	0.247	0.146	0.974	0.975
	kurt.	3.493	3.387	2.677	2.590	5.166	5.170
198	rms	0.124	0.117	0.111	0.111	0.125	0.125
	skew.	0.936	0.728	0.284	0.186	1.493	1.494
	kurt.	4.648	4.492	3.095	2.993	8.956	8.956
199	rms	0.069	0.066	0.065	0.064	0.069	0.069
	skew.	0.906	0.553	0.290	0.215	0.932	0.932
	kurt.	4.873	4.062	3.366	3.256	5.491	5.491

Note, rms error is in units of m/s, whereas skewness (skew.) and kurtosis (kurt.) are normalized dimensionless quantities.

Table 3-RMS Error of Predictions [m/s]

Run	Super.	Stret.	M.Stret.	Extrp.	Lin.
188	0.0590	0.0593	0.0593	0.1243	2.5274
189	0.0364	0.0364	0.0366	0.0749	0.2270
190	0.0378	0.0394	0.0399	0.0571	0.0731
191	0.0292	0.0294	0.0295	0.0359	0.0374
196	0.0548	0.0596	0.0616	0.0871	0.2214
197	0.0399	0.0425	0.0438	0.0419	0.0419
198	0.0413	0.0433	0.0443	0.0451	0.0451
199	0.0241	0.0253	0.0258	0.0235	0.0235

Figure Captions

Figure 1. Illustration of superpositon, showing a shorter wave riding on a longer wave.

Figure 2. DHH directional spectrum after Donelan *et al.* (1985) showing the value of the parameters employed to produce the time series of surface elevation used for the numerical simulation.

Figure 3 (a). Simulated time series showing surface elevation and the wave-induced velocities predicted by the various methods. **(b)** Enlargement of a segment of the time series shown in 3a.

Figure 4. Variation of the horizontal velocity (u) as a function of depth for the various methods.

Figure 5. Electro-hydraulic surface-follower device with Minilab SD-12 3-axis acoustic current meter attached.

Figure 6 (a). Response of the surface-follower to an irregular surface displacement. The solid line shows the water surface fluctuation, the dashed line shows the follower-piston position, and the dotted line shows the variation in the depth of immersion, (*i.e.*, the following error); note, all three quantities are plotted to the same scale. **(b)** Transfer function of the surface-follower, showing the amplitude and frequency response as a function of frequency.

Figure 7.(a) Along axes response for the x and y channels of the Minilab SD-12 acoustic current meter showing the instrument linearity. **(b)** Horizontal (x-y) gain cosine response of x-y axes with respect to the gain at 0° (*i.e.*, the along-axis gain). The dashed line is the expected cosine response.

Figure 8. Measured velocity (solid line) with that predicted by superposition (dashed line) and stretching (dotted line) for a short segment of run 188 **(a)**, run 191 **(b)**, and run 196 **(c)**.

Figure 9. Scatter plot of measured velocity at 46 mm beneath the free surface versus that predicted using **(a)** superposition, **(b)** stretching, **(c)** modified stretching, and **(d)** extrapolation for run 188.

Figure 10. Scatter plot of measured velocity at 126 mm beneath the free surface versus that predicted using **(a)** superposition, **(b)** stretching, **(c)** modified stretching, and **(d)** extrapolation for run 196.

Figure 11. Scatter plot of measured velocity at 46 mm beneath the free surface versus that predicted using **(a)** superposition, **(b)** stretching, **(c)** modified stretching, and **(d)** extrapolation for run 191.

Figure 12. Spectrum of measured velocity (——) and that predicted using superposition (- - - -) and stretching (···) for runs 188 **(a)**, 191 **(b)**, and 196 **(c)**. $\delta f = 0.104$ Hz and there are 16 degrees of freedom.

Figure 1

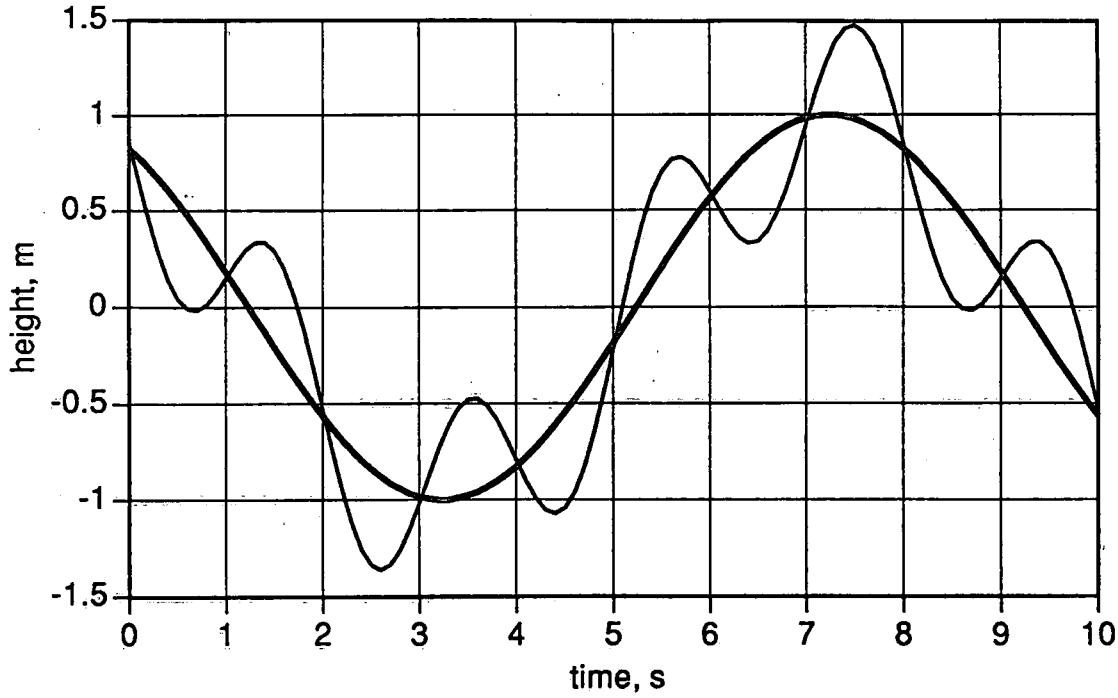

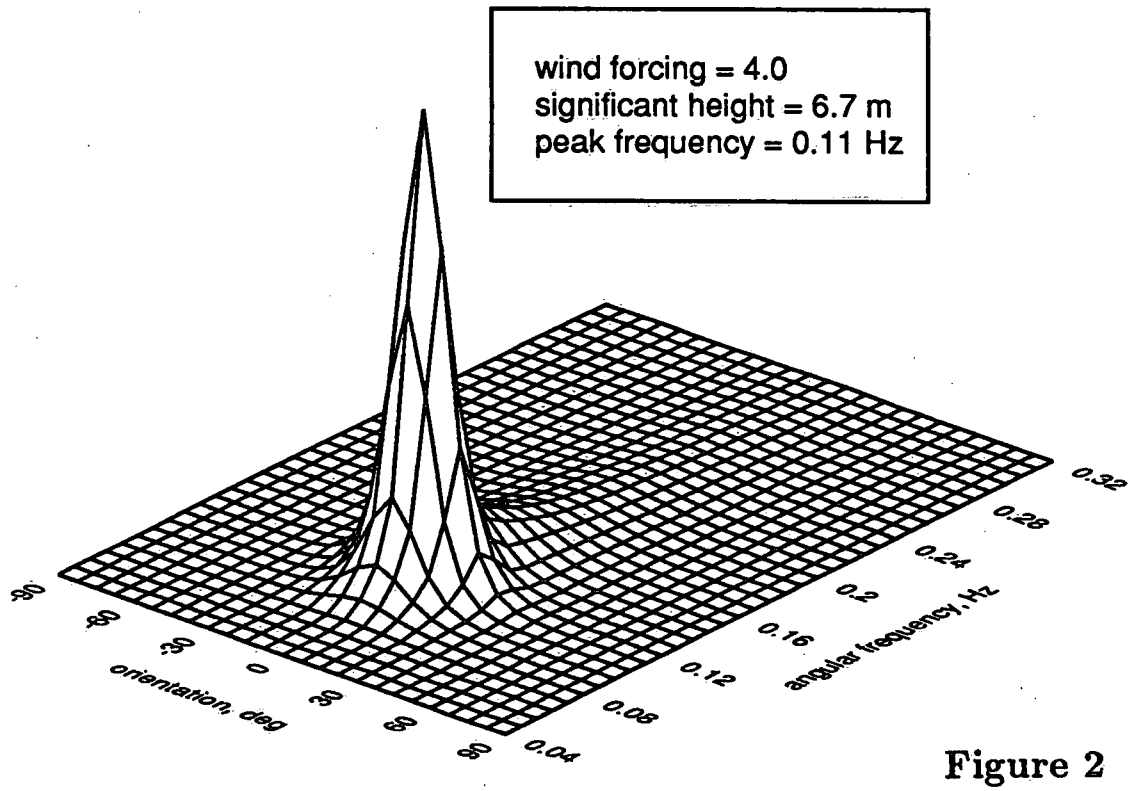

Figure 2

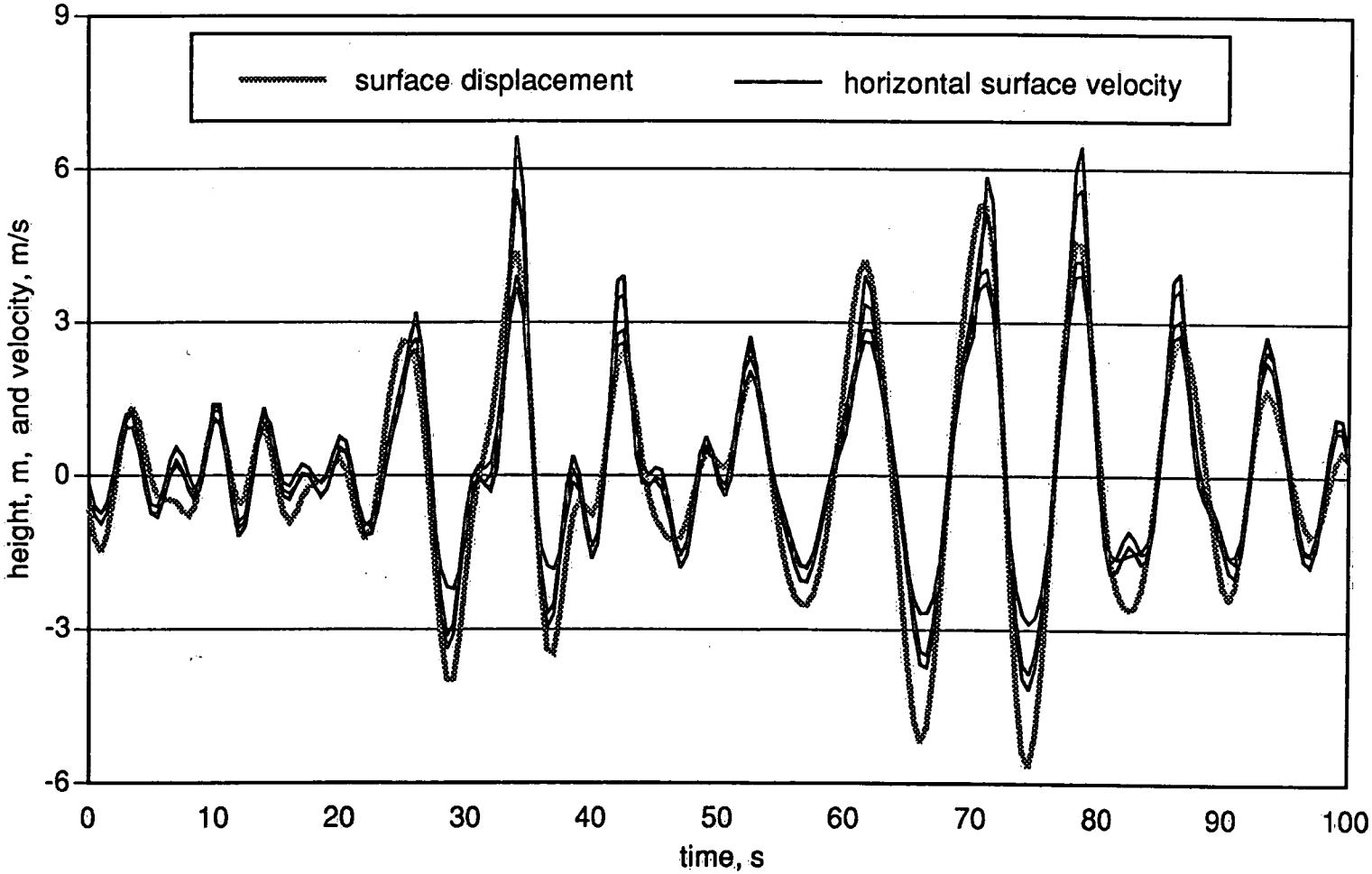
surface displacement
horizontal surface velocity
height, m, and velocity, m/s
time, s
9
6
3
0
-3
-6
0
10
20
30
40
50
60
70
80
90
100

Figure 3(a)

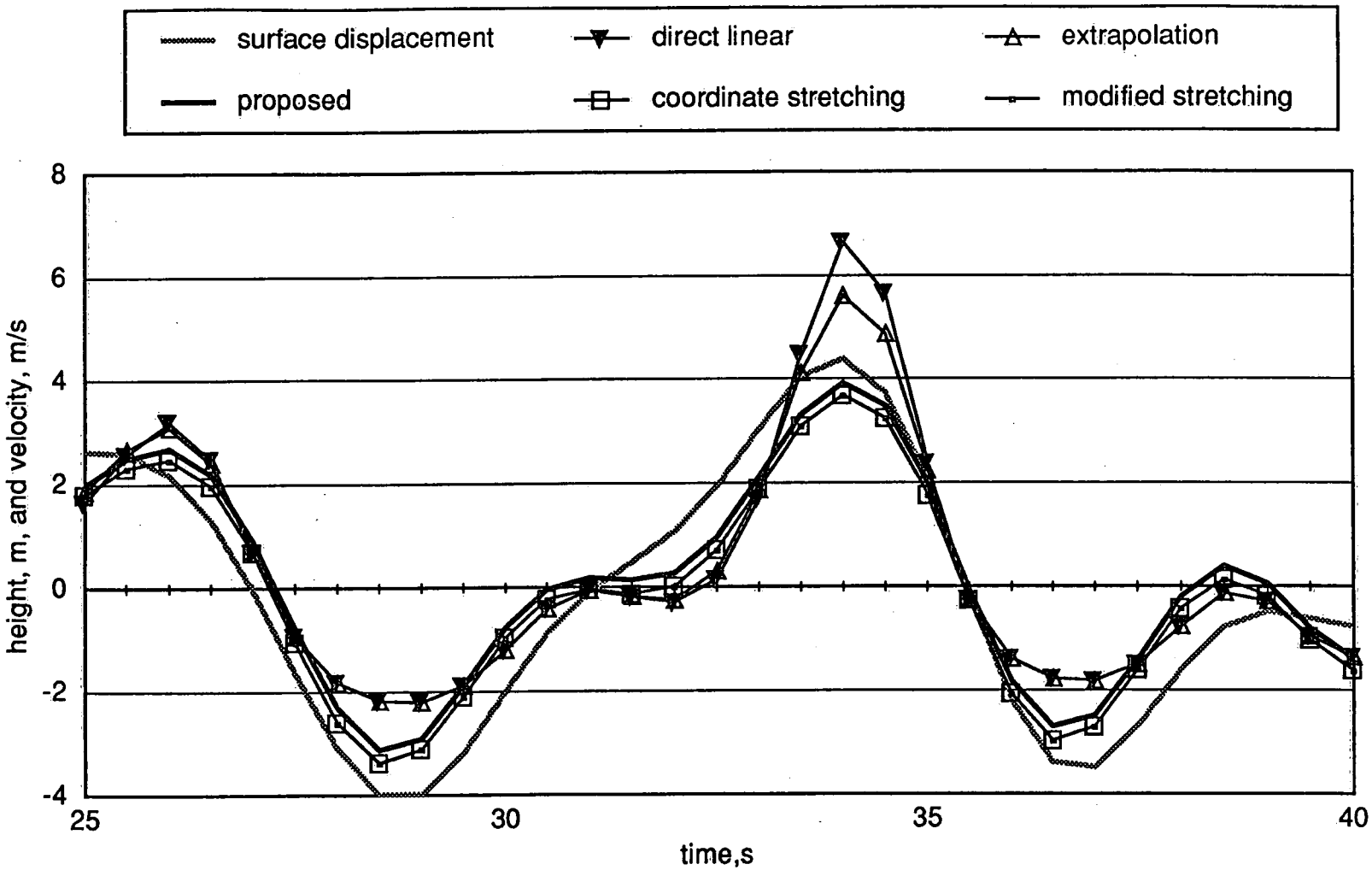
surface displacement
direct linear
extrapolation
proposed
coordinate stretching
modified stretching
height, m, and velocity, m/s
8
6
4
2
0
-2
-4
25
30
35
40
time,s

Figure 3(b)

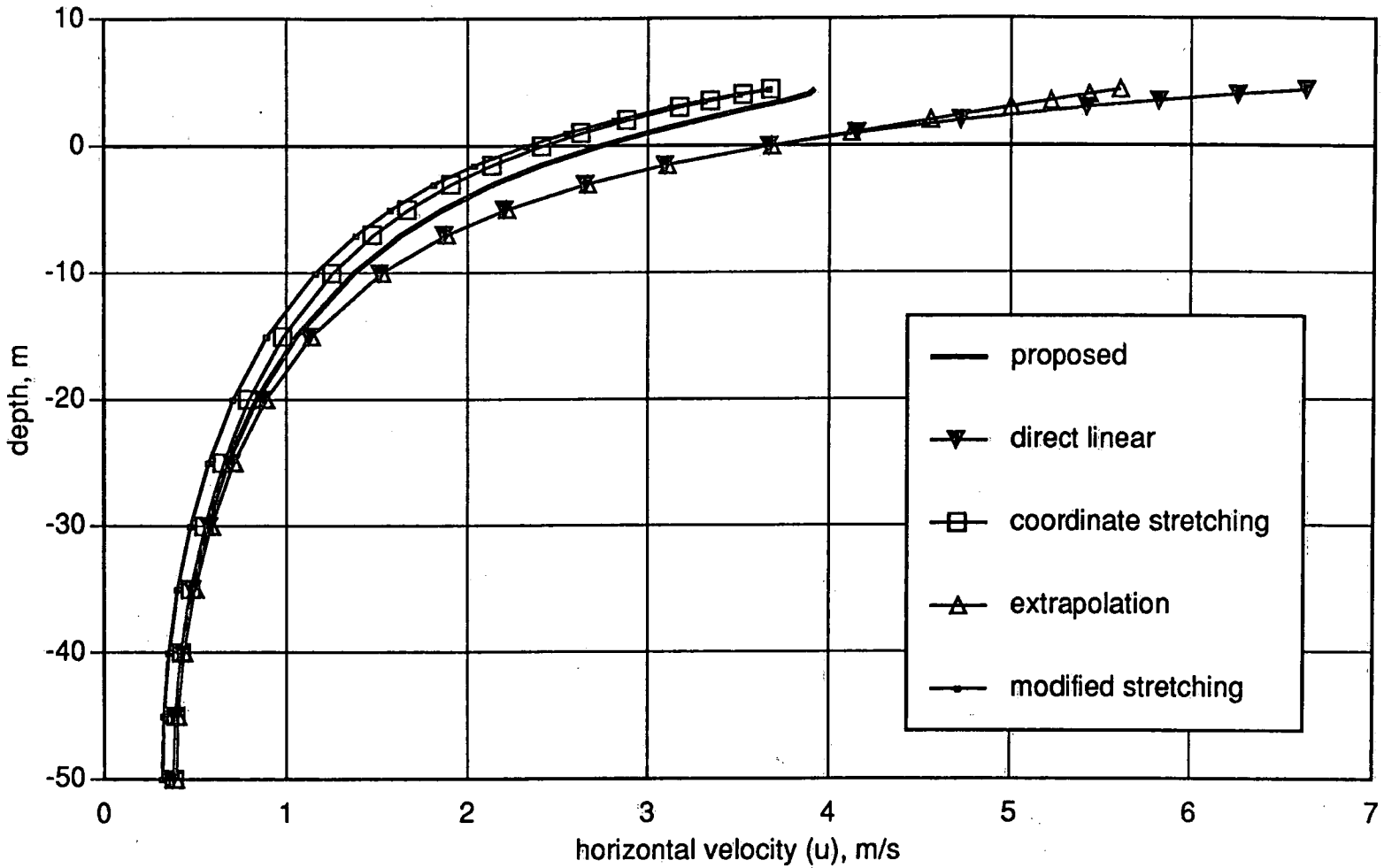
10
0
-10
-20
-30
-40
-50
depth, m
0
1
2
3
4
5
6
7
horizontal velocity (u), m/s
proposed
direct linear
coordinate stretching
extrapolation
modified stretching

Figure 4

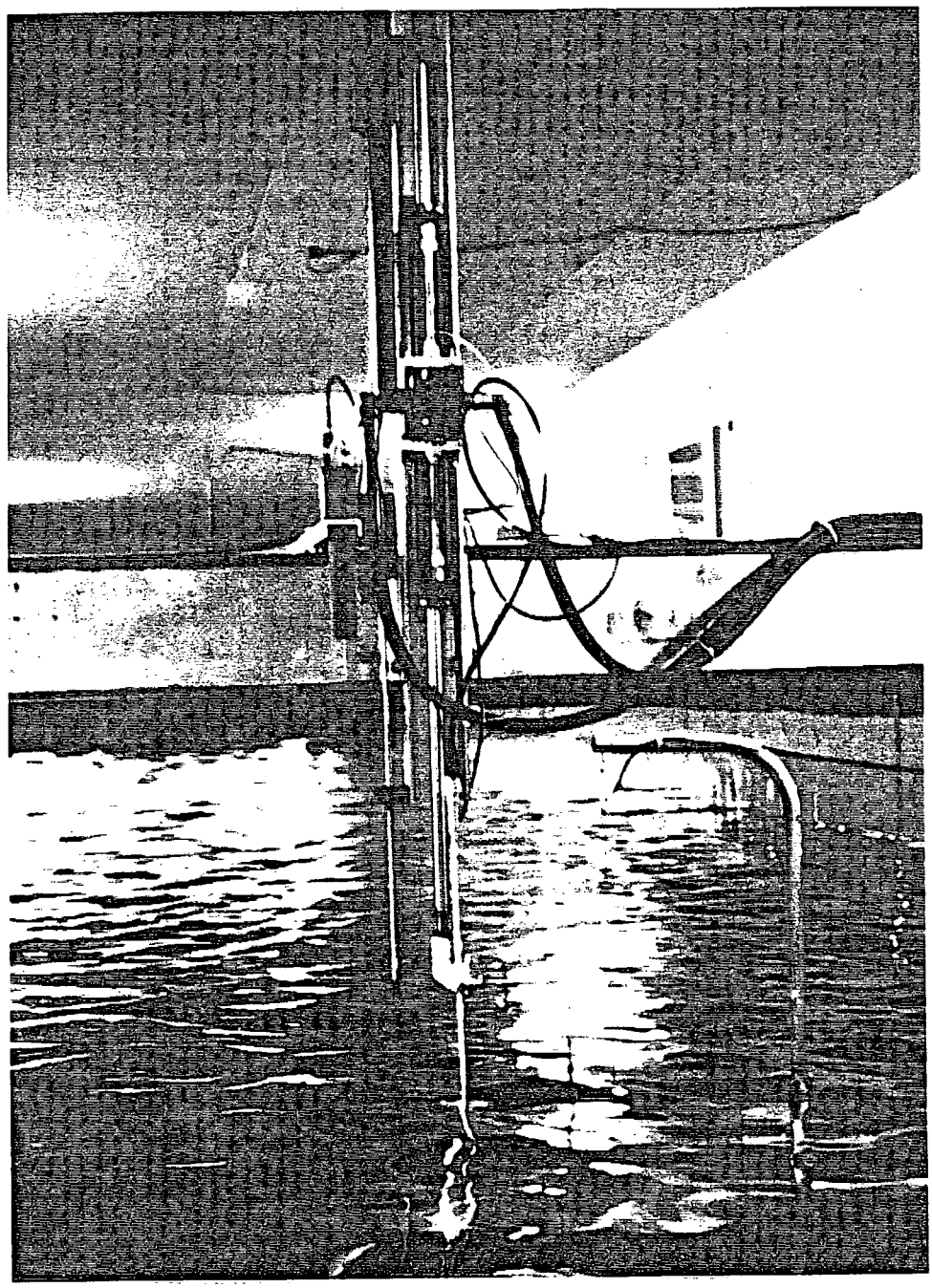

Figure 5

Figure 6(a)

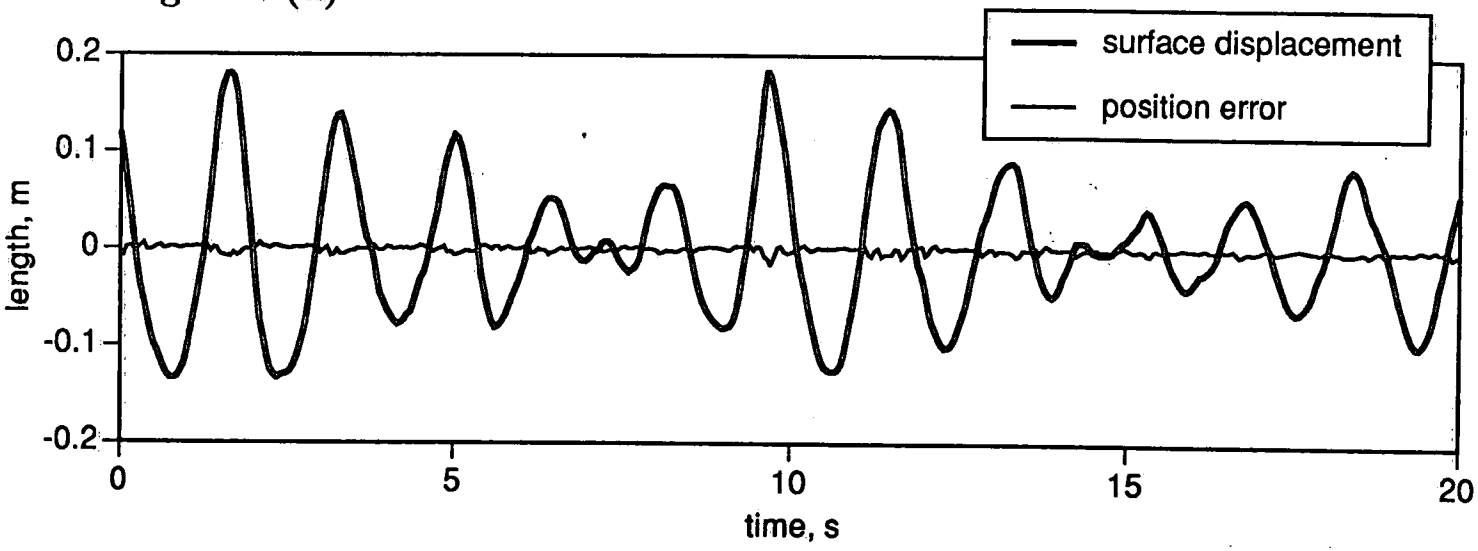

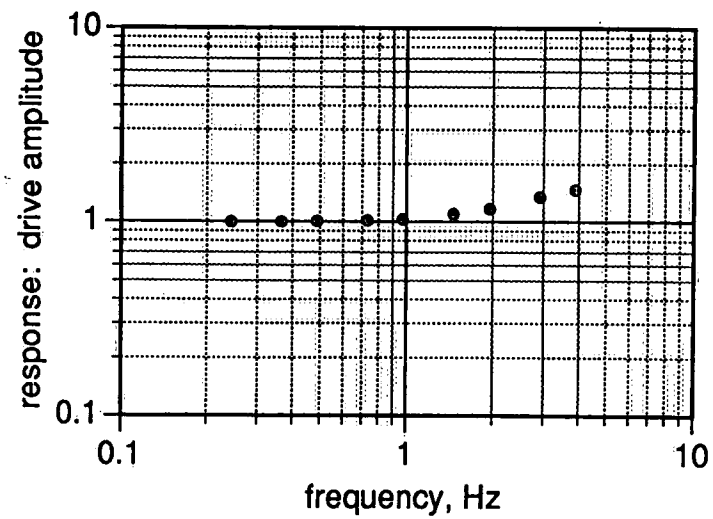

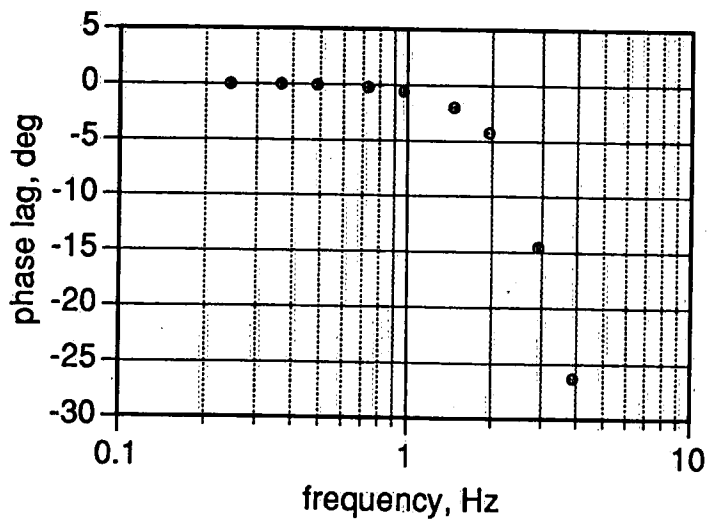

Figure 6(b)

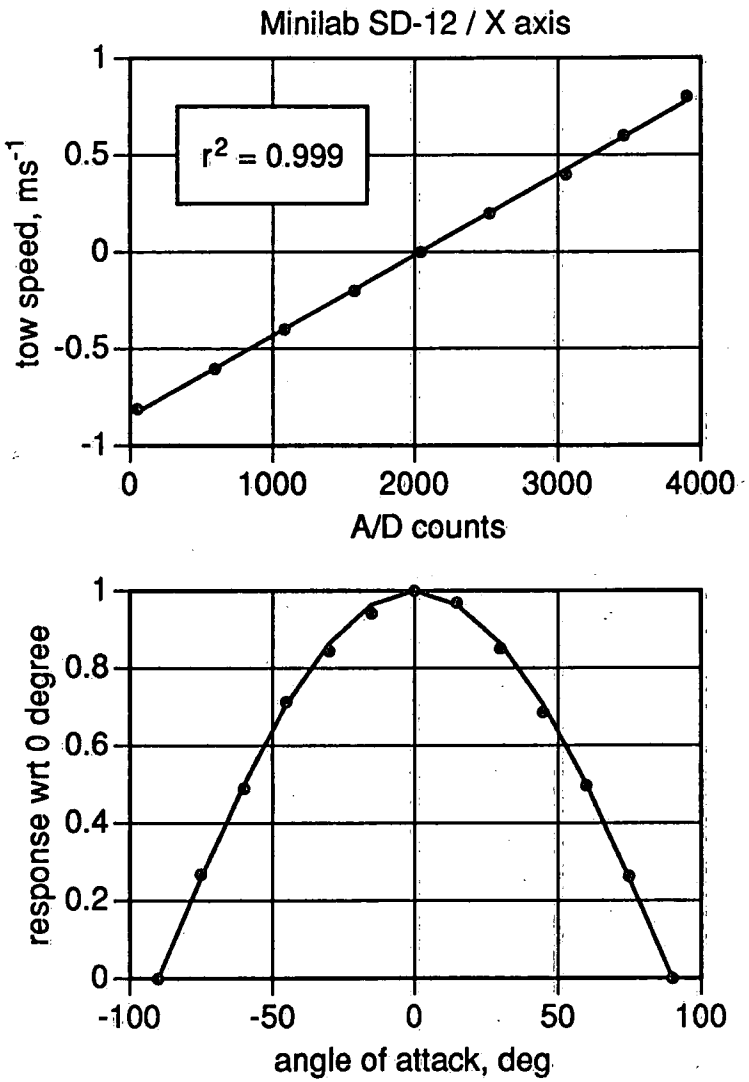

Figure 7(a)

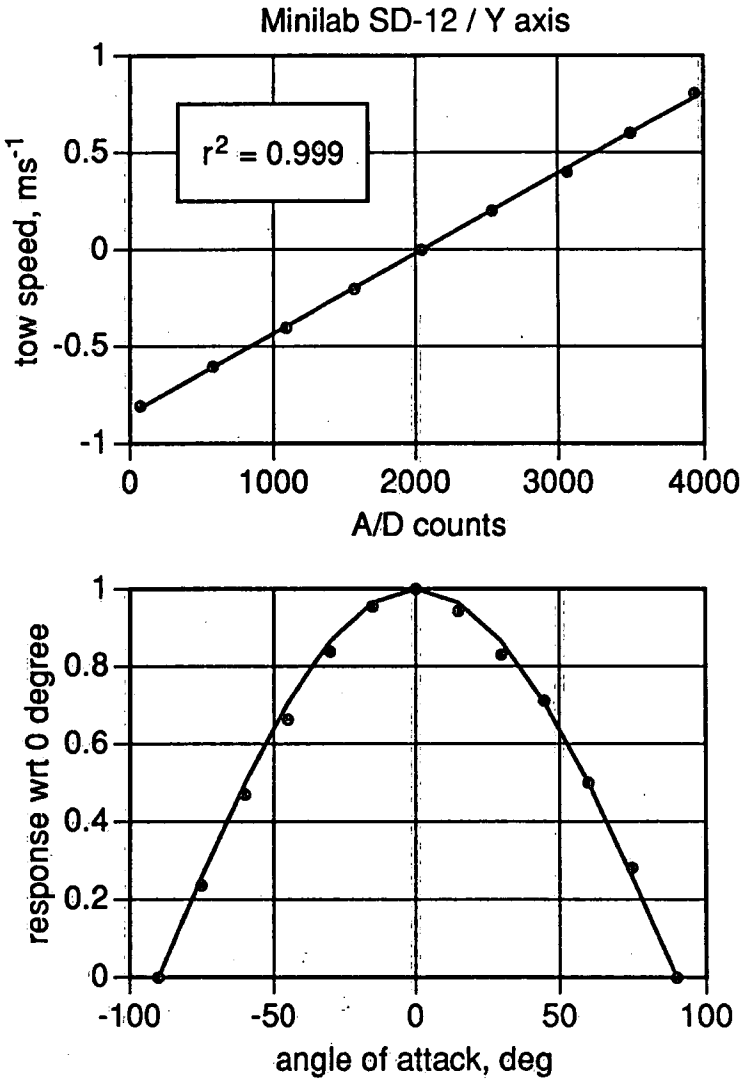

Figure 7(b)

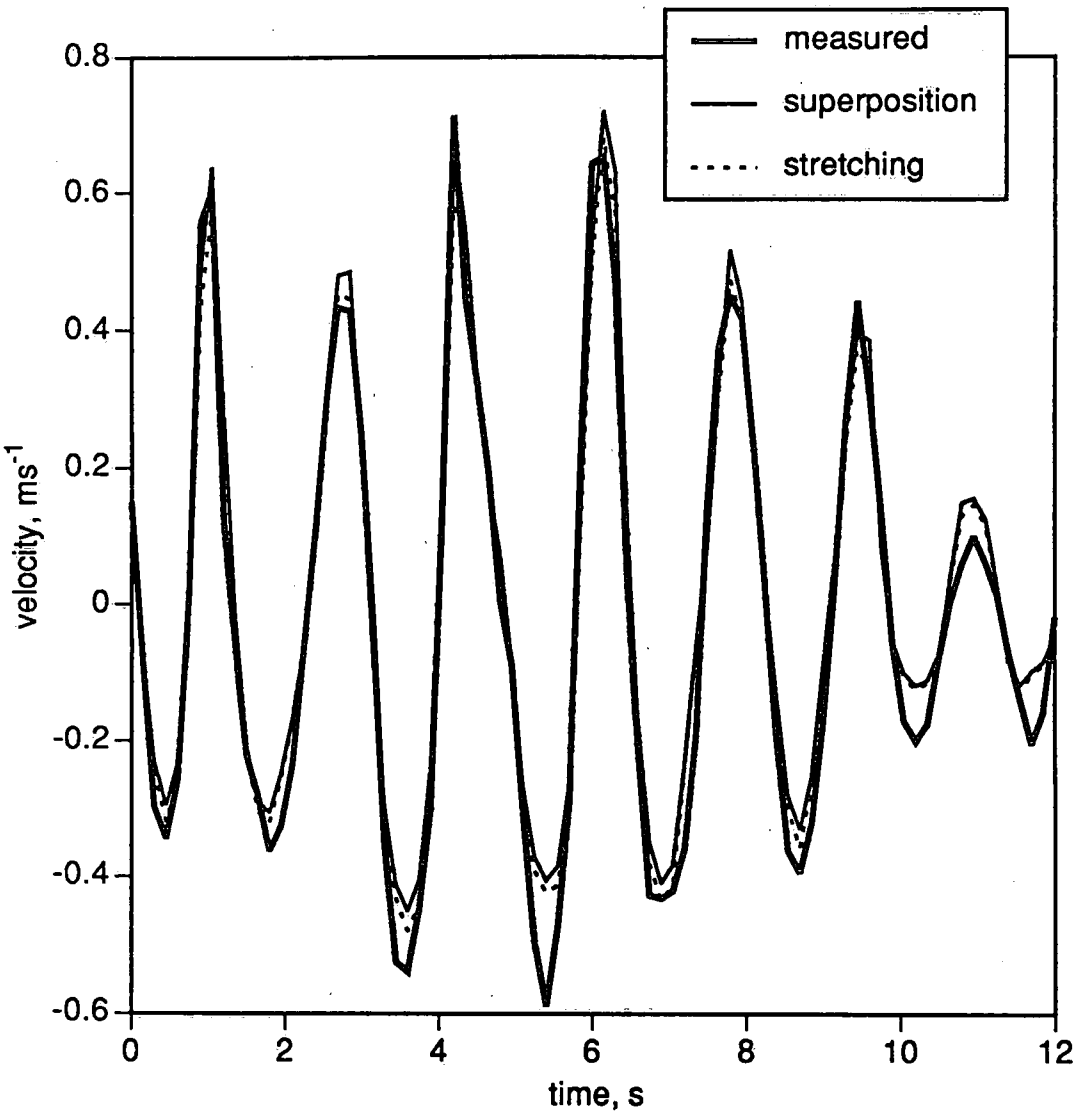
measured
superposition
stretching
0.8
0.6
0.4
0.2
0
-0.2
-0.4
-0.6
velocity, ms-1
0
2
4
6
8
10
12
time, s

Figure 8(a)

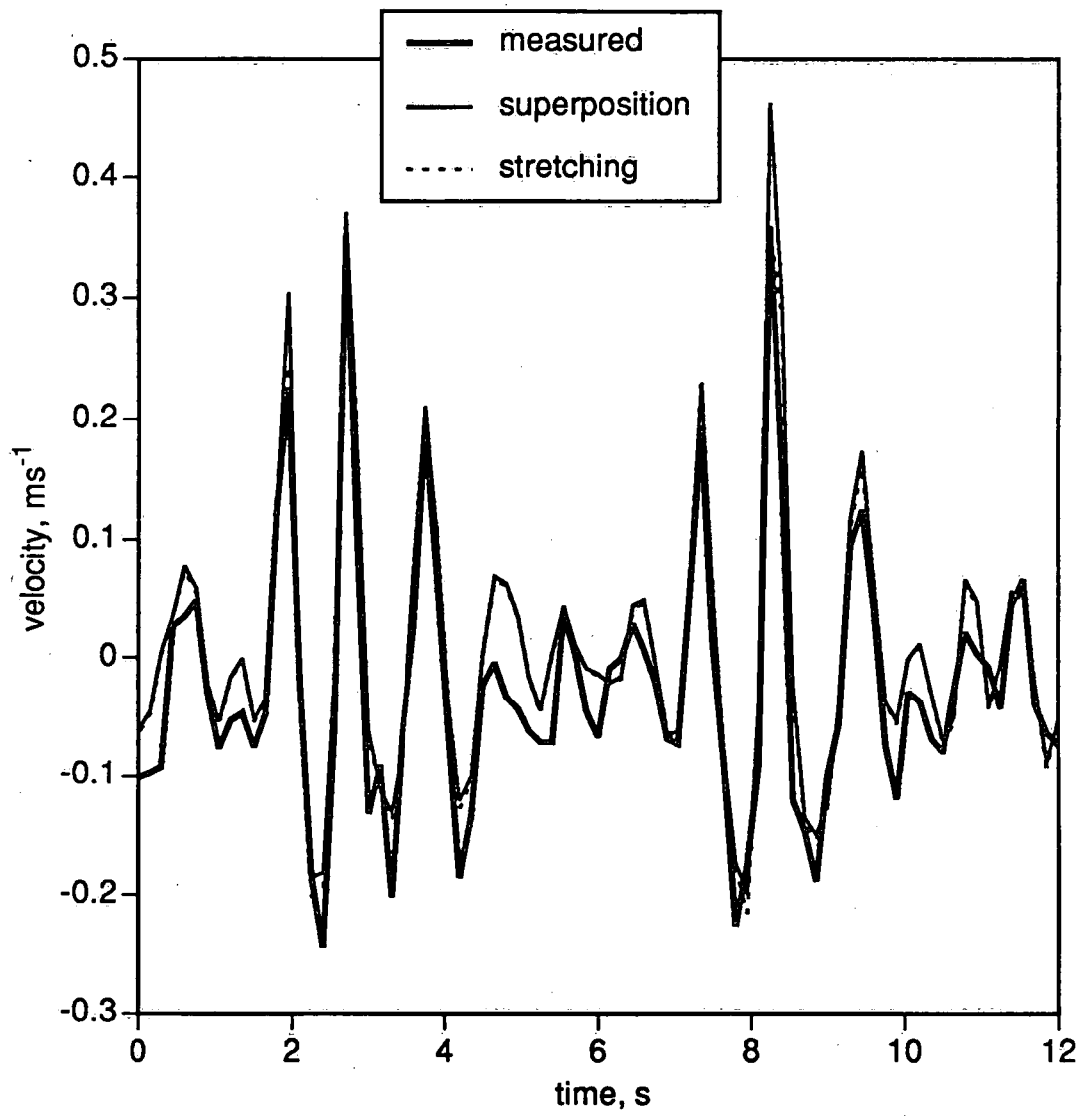
measured
superposition
stretching
0.5
0.4
0.3
0.2
0.1
0
-0.1
-0.2
-0.3
velocity, ms-1
0
2
4
6
8
10
12
time, s

Figure 8(b)

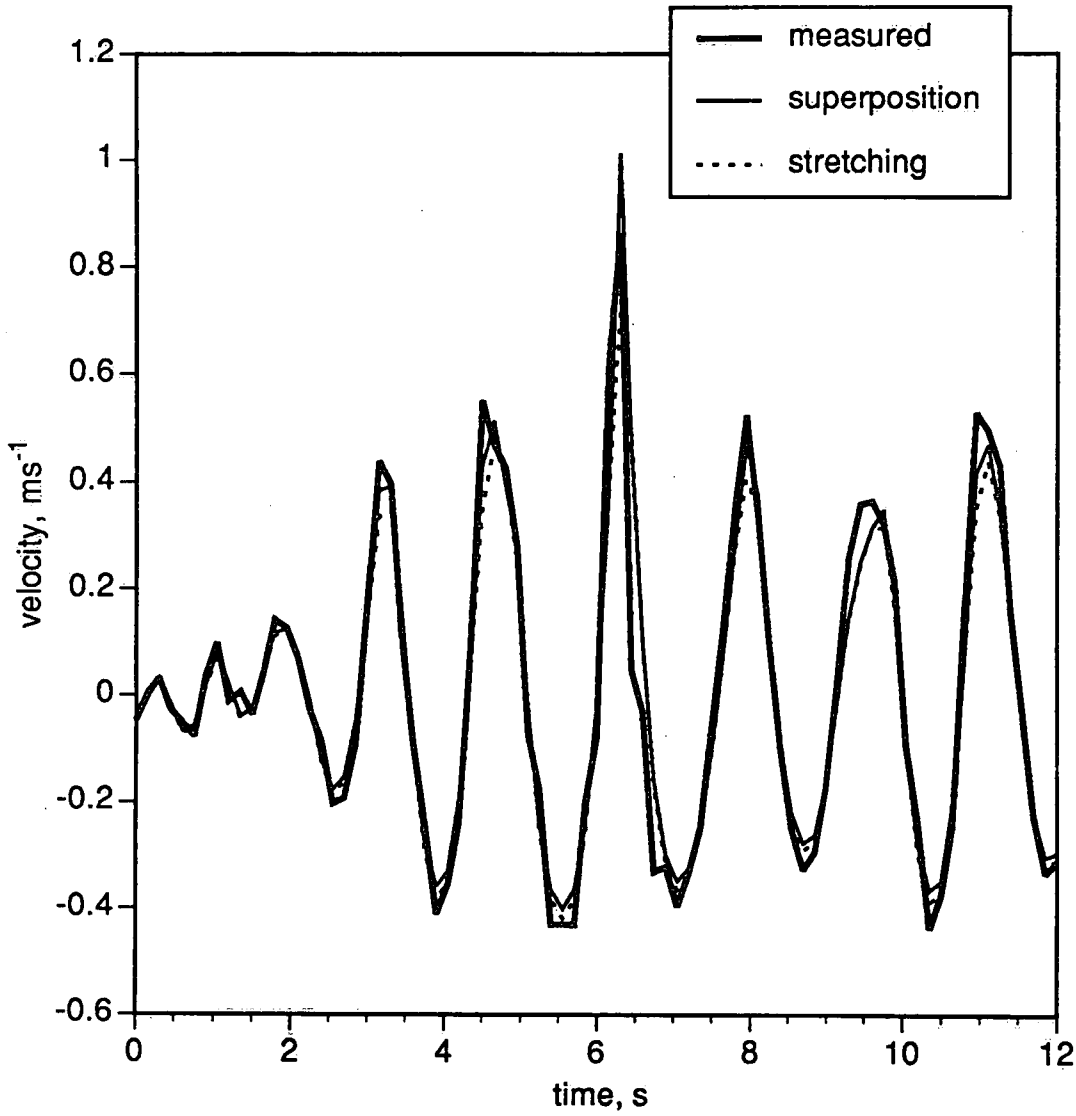
measured
superposition
stretching
1.2
1
0.8
0.6
0.4
0.2
0
-0.2
-0.4
-0.6
velocity, ms-1
0
2
4
6
8
10
12
time, s

Figure 8(c)

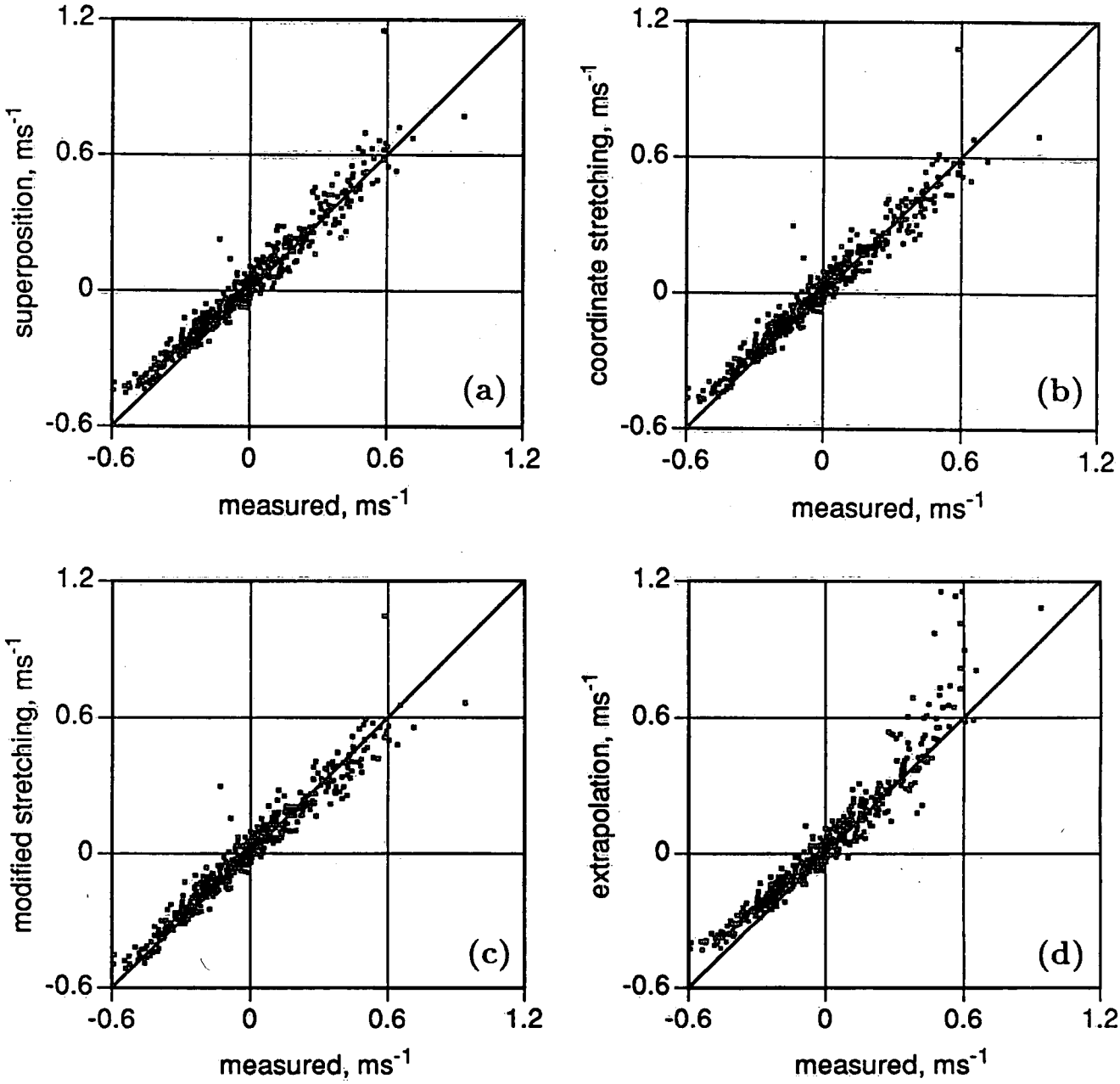
1.2
0.6
0
-0.6
superposition, ms-1
(a)
-0.6
0
0.6
1.2
measured, ms-1
coordinate stretching, ms-1
(b)
modified stretching, ms-1
(c)
extrapolation, ms-1
(d)

Figure 9

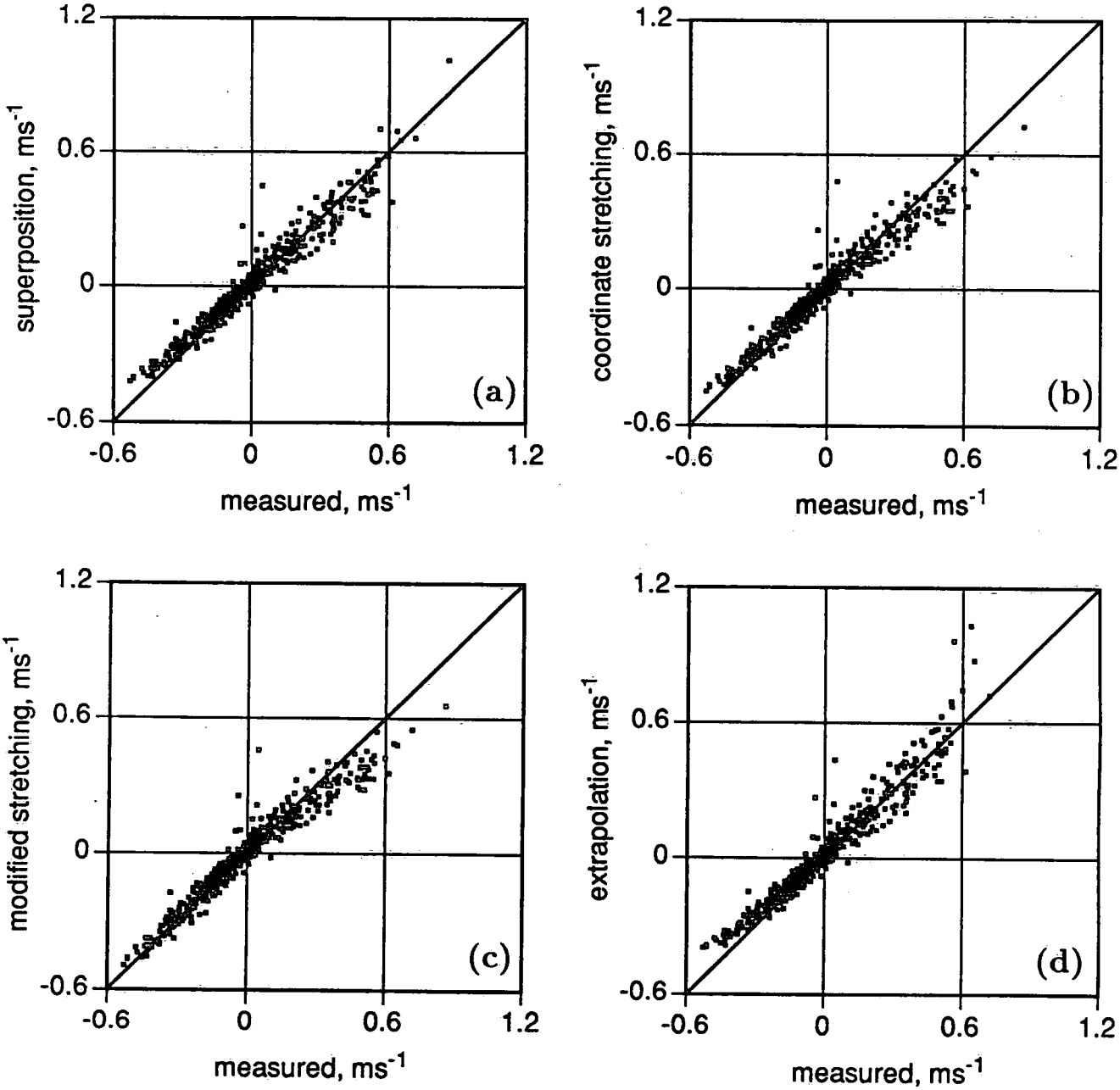
1.2
0.6
0
-0.6
superposition, ms-1
(a)
-0.6
0
0.6
1.2
measured, ms-1
coordinate stretching, ms-1
(b)
modified stretching, ms-1
(c)
extrapolation, ms-1
(d)

Figure 10

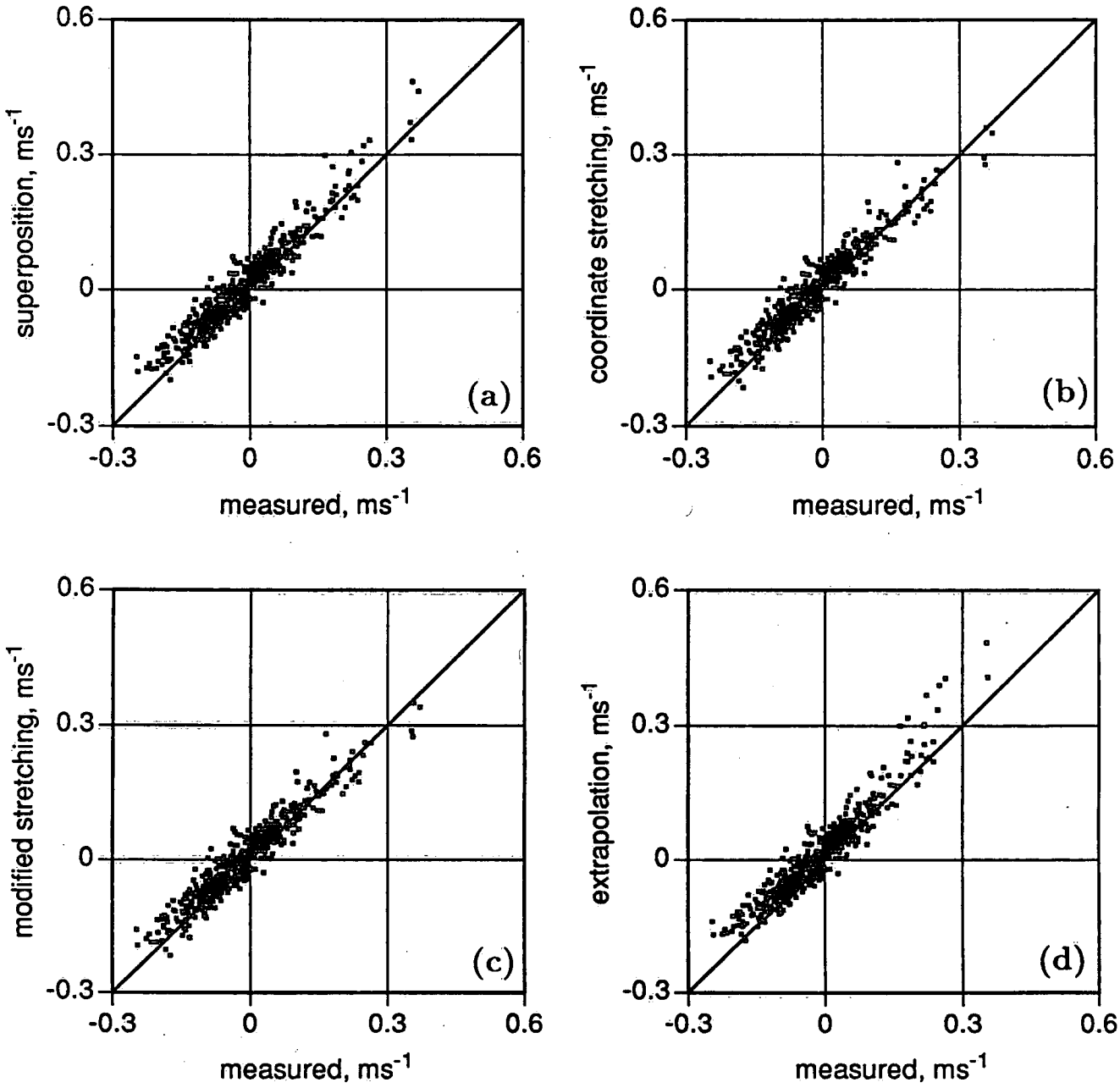
0.6
0.3
0
-0.3
superposition, ms-1
measured, ms-1
(a)
coordinate stretching, ms-1
(b)
modified stretching, ms-1
(c)
extrapolation, ms-1
(d)

Figure 11

Figure 12(a)

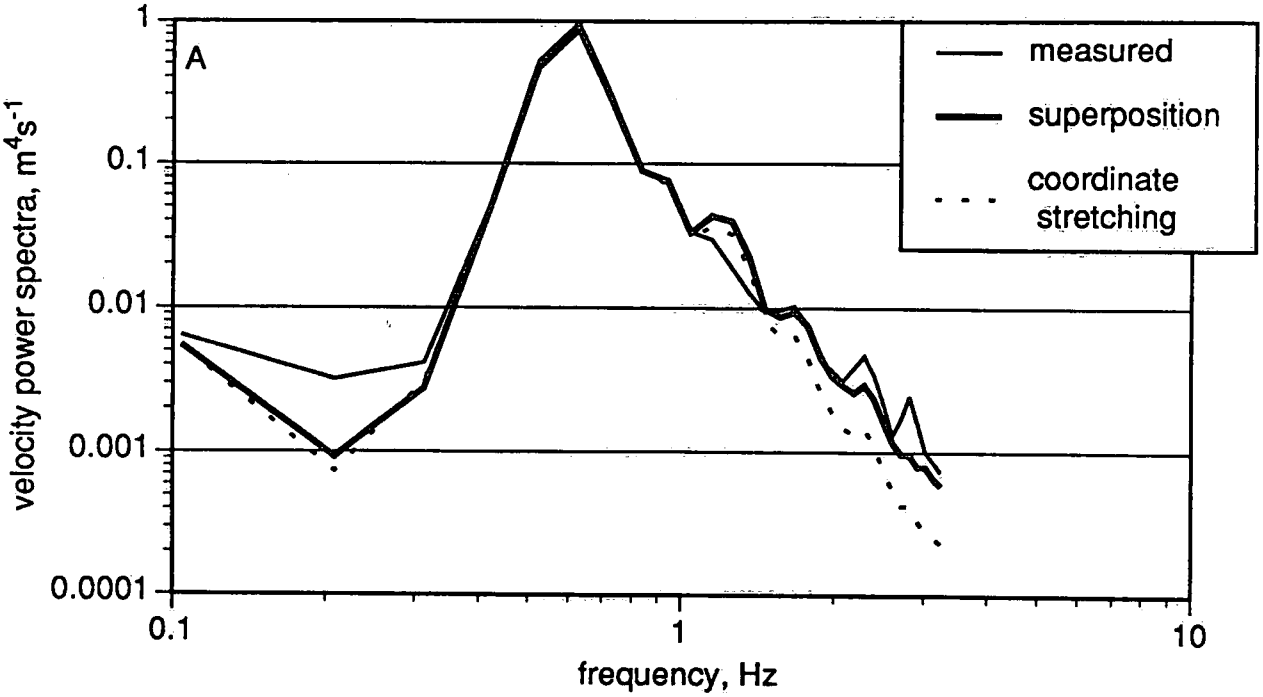

Figure 12(b)

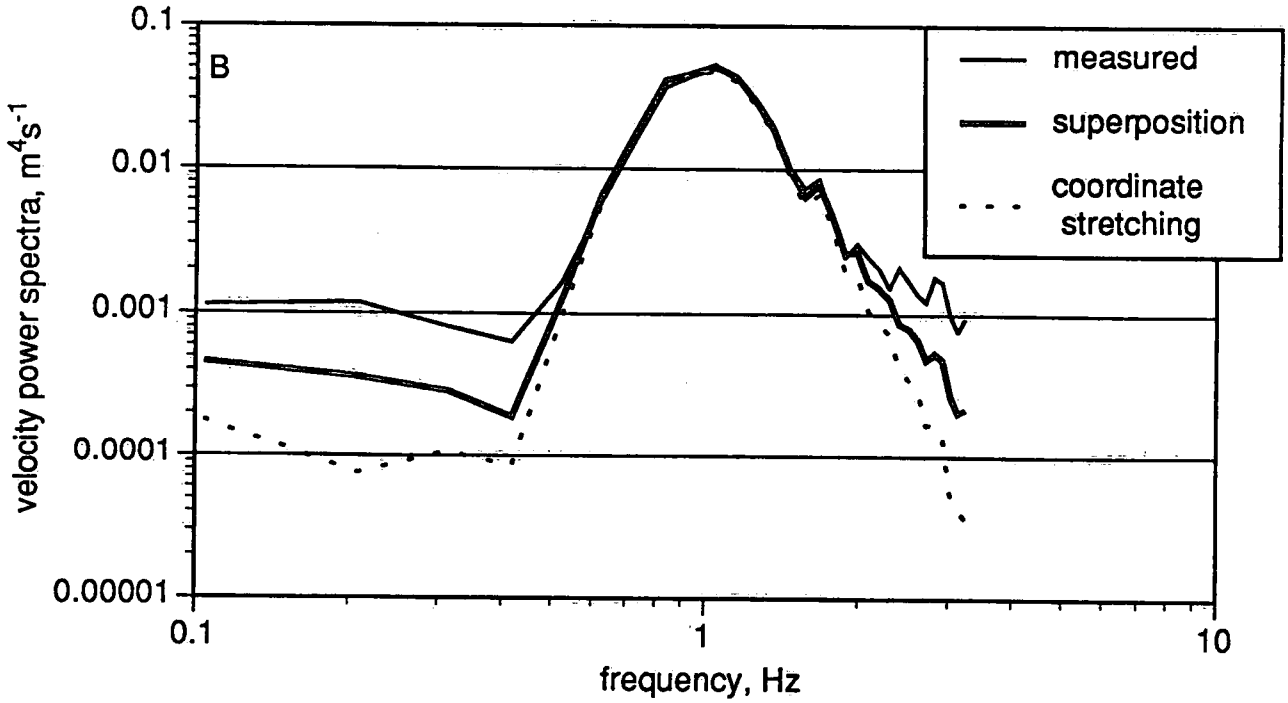

Figure 12(c)

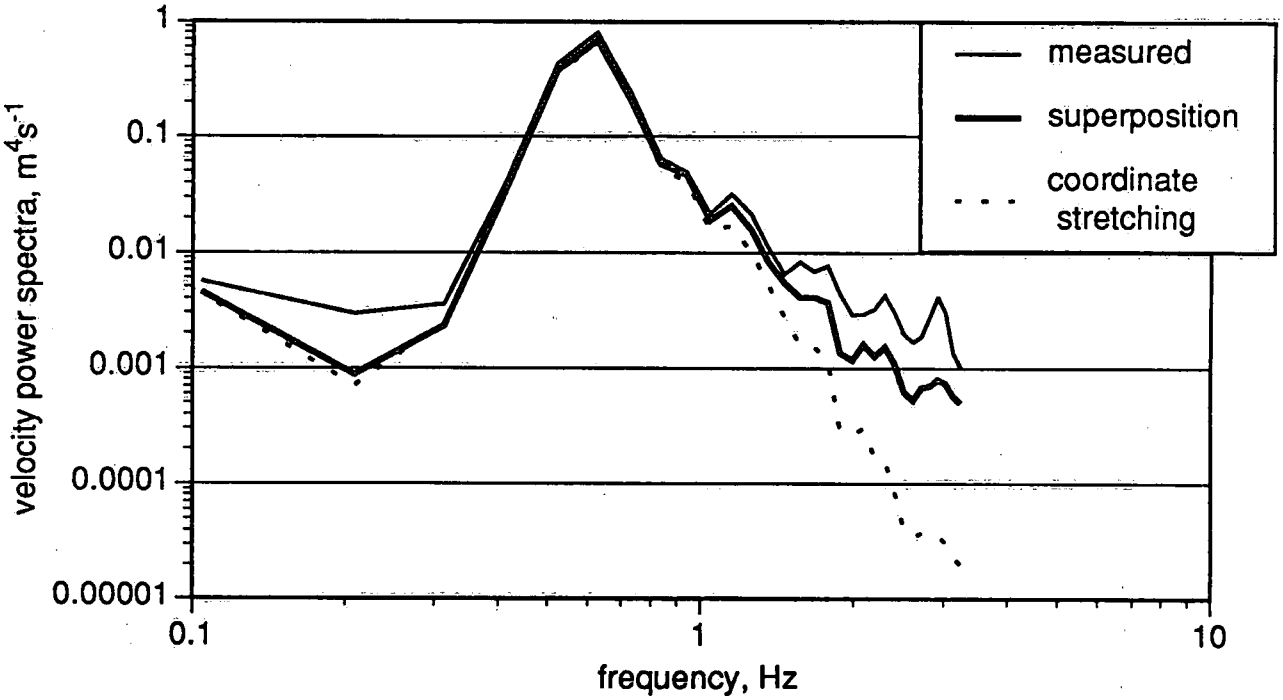
1
0.1
0.01
0.001
0.0001
0.00001
velocity power spectra, m4s-1
0.1
1
10
frequency, Hz
measured
superposition
coordinate stretching

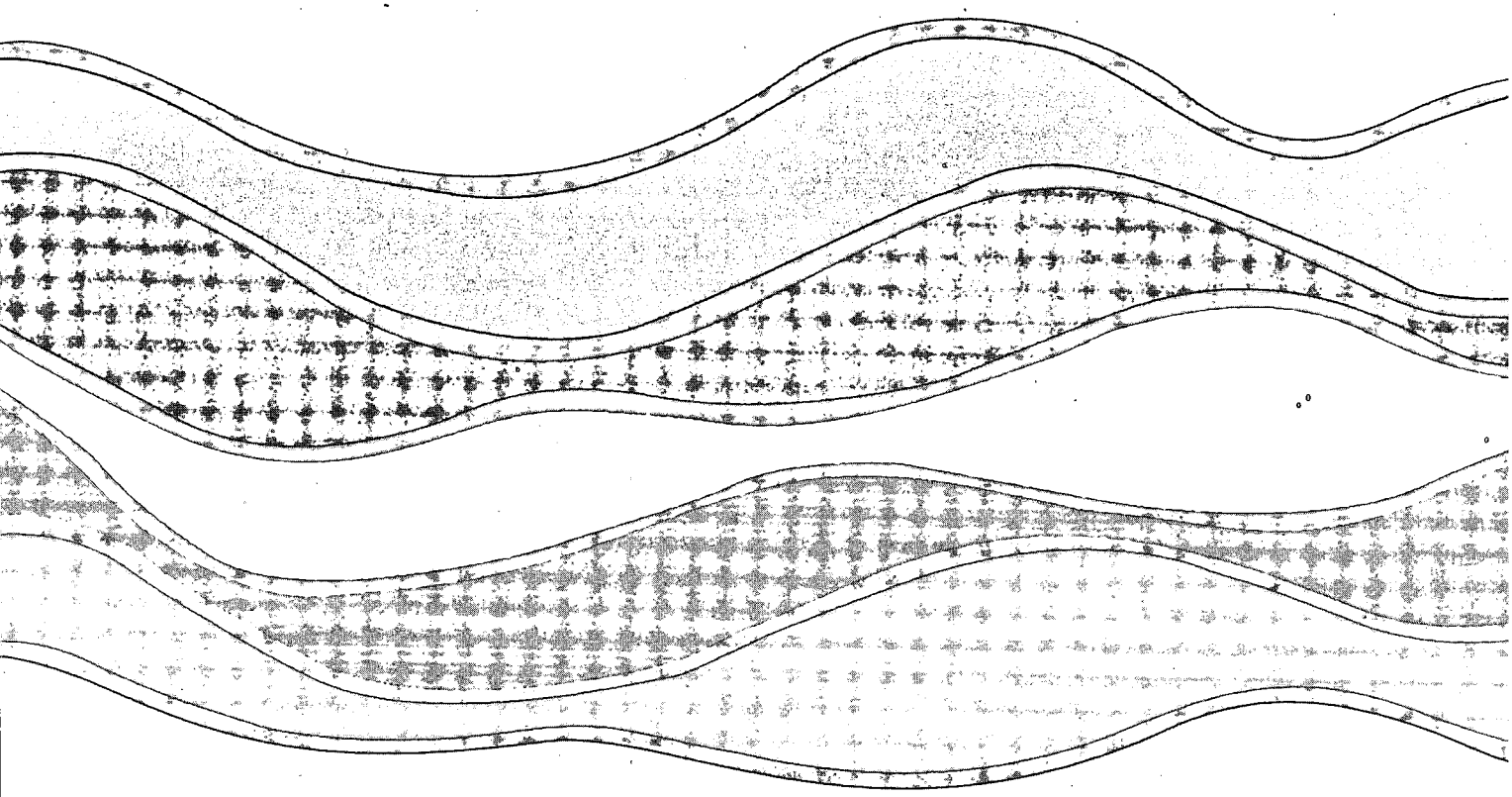

NATIONAL WATER RESEARCH INSTITUTE
P.O. BOX 5050, BURLINGTON, ONTARIO L7R 4A6

Environment Canada Environnement Canada

Canada

INSTITUT NATIONAL DE RECHERCHE SUR LES EAUX
C.P. 5050, BURLINGTON (ONTARIO) L7R 4A6